Kaunas University of Technology
Faculty of Mathematics and Natural Sciences

Dosimetric impact of planning volume distinction observed in different strategies of lung SBRT

Master's Studies Final Project

Project prepared by
Akvilė Kuncytė

Project supervisor
Assoc. prof. Evelina Jaselskė

Kaunas, 2026

Kaunas University of Technology

Faculty of Mathematics and Natural Sciences

Dosimetric impact of planning volume distinction observed in different strategies of lung SBRT

Master's Studies Final Project

Medical Physics (6213GX001)

Project prepared by

Akvilė Kuncytė

Project supervisor

Assoc. prof. Evelina Jaselskė

Project reviewed by

Assoc. prof. Linas Puodžiukynas

Kaunas, 2026

Kaunas University of Technology

Faculty of Mathematics and Natural Sciences

Akvilė Kuncytė

Dosimetric impact of planning volume distinction observed in different strategies of lung SBRT

Declaration of academic integrity

I confirm that:

1. I have prepared this final project independently and honestly, without violating the copyright or other rights of other persons, in compliance with the Law on Copyright and Related Rights of the Republic of Lithuania, the provisions of Kaunas University of Technology (hereinafter referred to as the University) on the management and transfer of intellectual property, and the ethical requirements set out in the University's Code of Academic Ethics;

2. All data and research results presented in the final project are accurate and obtained legally, no part of the project has been plagiarised from printed or electronic sources, and all quotations and references presented in the text of the final project are indicated in the list of references;

3. I have complied with personal data protection requirements in the final project, have not used undisclosed or confidential data without legal grounds, and if I have used such data, it has been properly anonymised;

4. If I used artificial intelligence (hereinafter referred to as AI) or other automated tools in preparing the final project, I applied them in accordance with the procedures established by the University, without violating the principles of academic integrity.

5. I have not paid and am not obliged to pay any sums of money not provided for by law for the final project or any part thereof to any natural or legal person;

6. I understand that if academic dishonesty or violation of other persons' rights is discovered, I will be held accountable in accordance with the procedures established by the University and may be expelled from the University; cases of academic dishonesty may be investigated even after graduation, initiating the procedure for revoking the degree.

Kuncytė, Akvilė. Dosimetric impact of planning volume distinction observed in different strategies of lung SBRT. Master's Final Degree Project of Medical Physics / supervisor assoc. prof. Evelina Jaselskė; Faculty of Mathematics and Natural Sciences, Kaunas University of Technology.

Field of study and group of fields of study: Medical Technologies (Health Sciences)

Keywords: lungs, SBRT, MRgART, 4D-CT, respiratory motion management.

Kaunas, 2026. 60 pages.

Summary

Globally, lung cancer remains one of the most common causes of cancer occurrence and mortality. Stereotactic body radiation therapy has grown in importance as a therapeutic option for early-stage lung cancer due to the disease's rising clinical occurrence. The treatment modality inevitably requires precise target definition and motion management, as even slight changes in planning target volume can significantly affect dosimetric quality and normal tissue sparing.

This study focuses on the increasing significance of dosimetric optimization in lung stereotactic body radiation therapy with four-dimensional computed tomography and the growing implementation of magnetic resonance-guided adaptive radiation technologies in thoracic oncology, which shape new options for margin reduction and motion management.

The aim of the study is to evaluate and compare the structures of the planned target volume across lung radiotherapy methods implemented with different radiotherapy equipment and to determine their impact on clinical outcomes. The work tasks include: 1) a scientific review of lung stereotactic body radiotherapy, focusing on treatment planning principles in thoracic radiotherapy; 2) evaluation and comparison of the dosimetric characteristics of lung stereotactic radiotherapy strategies; 3) analysis of differences in the planning target volume between conventional and stereotactic radiotherapy methods by developing a statistical modulation.

In this study, statistical analysis methods were applied to evaluate lung stereotactic body radiotherapy planning strategies. Target volume parameters and dose-volume histogram metrics were analyzed and compared across different planning approaches using correlation and linear regression analyses. Statistical modeling methods were focused on differences in the planned target content using uniform margins and principal component analysis.

Comparison between stereotactic methods and dose-volume metrics has been complicated by differing implied clinical criteria, which are more stringent in the magnetic resonance-guided adaptive radiotherapy (MRgART) strategy. However, the analysis demonstrated that a higher chest wall dose was significantly associated with increased planning target volume (PTV) maximum dose ($p = 0.007$), suggesting that relaxing chest wall constraints may permit greater dose escalation within the target volume. The maximum chest wall dose also showed a positive association with PTV $D_{98\%}$ coverage, suggesting a potential trade-off between improved target

coverage and increased chest wall irradiation. In contrast, Lung-GTV showed a significant negative relationship ($p = 0.044$) with PTV maximum dose, indicating that stricter lung dose limitations may restrict achievable target hotspot intensity. The stereotactic MRgART method, which, in a statistical modeling investigation, attained an expansion value of 24.19 at a 10 mm verge—more than double the 5 mm margin—can be seen as the most sensitive method for margin expansion.

This study highlights that motion management strategies including 4D-CT, respiratory gating, and MR-guided adaptive radiotherapy are crucial for lowering motion uncertainty, minimizing PTV margins, and enhancing dosimetric precision since respiratory motion has a major impact on lung radiation planning. Moreover, stricter lung sparing seemed to restrict dose escalation within the target volume, while improved target coverage was linked to higher chest wall dose. Nonetheless, smaller target volumes showed higher relative geometric growth, according to statistical modeling, which may increase irradiation of nearby healthy lung tissue.

Kuncytė, Akvilė. Planavimo tūrio dozimetrinis poveikis, taikant skirtingas plaučių SBRT strategijas. Medicinos Fizikos magistro baigiamasis projektas / vadovė assoc. prof. Evelina Jaselskė; Kauno technologijos universitetas, Matematikos ir gamtos mokslų fakultetas.

Studijų kryptis ir studijų krypčių grupė: Medicinos technologijos (Sveikatos mokslai)

Reikšminiai žodžiai: plaučiai, SBRT, MRgART, keturių dimensijų kompiuterinė tomografija (4D-KT), kvėpavimo judesių valdymas.

Kaunas, 2026. 60 p.

Santrauka

Pasauliniu mastu plaučių vėžys išlieka viena dažniausių vėžio atsiradimo ir mirtingumo priežasčių. Stereotaksinės kūno radiaterapijos, atveriančios galimybę ankstyvos stadijos plaučių vėžiui gydyti, svarba išaugo dėl didėjančio ligos klinikinio paplitimo. Spindulinis gydymo būdas neišvengiamai reikalauja tikslaus taikinio apibrėžimo ir judesių valdymo, nes net ir nedideli planuojamo taikinio tūrio pokyčiai gali reikšmingai paveikti dozimetrinę kokybę ir normalių audinių išsaugojimą.

Šiame tyrime daugiausia dėmesio skiriama didėjančiai dozimetrinio optimizavimo svarbai plaučių stereotaksinės kūno spindulinės terapijos metu naudojant keturių dimensijų kompiuterinę tomografiją ir didėjančiu magnetinio rezonanso valdomos adaptyviosios spinduliuotės technologijos pasitelkimu krūtinės ląstos onkologijoje, išsiskiriančiu planuojamojo taikinio tūrio paraščių mažinimo ir nauja judesių valdymo galimybe.

Šio tyrimo tikslas yra įvertinti ir palyginti planuojamo taikinio tūrio struktūras, taikant skirtingus plaučių spindulinės terapijos metodus bei spindulinės terapijos įrangą, ir nustatyti jų poveikį klinikiniams rezultatams. Darbo užduotys apima: 1) mokslinę plaučių stereotaksinės kūno spindulinės terapijos literatūros apžvalgą, skiriant dėmesį į gydymo planavimo principams krūtinės ląstos spindulinės terapijos srityje; 2) plaučių stereotaksinės spindulinės terapijos strategijų dozimetrinių charakteristikų vertinimą ir palyginimą; 3) planuojamo taikinio tūrio skirtumų tarp įprastinių ir stereotaksinės spindulinės terapijos metodų analizę, sukuriant statistinį modelį.

Tyrime buvo taikomi statistinės analizės metodai plaučių stereotaksinės kūno spindulinės terapijos planavimo strategijoms įvertinti. Taikinio tūrio parametrai ir dozės-tūrio histogramos metrikos buvo analizuojamos ir palyginamos taikant skirtingus planavimo metodus, naudojant koreliacijos ir tiesinės regresijos analizę. Statistinio modeliavimo atskleidimo metodai buvo orientuoti į planuojamo taikinio tūrio skirtumus, naudojant vienodas paraštes ir pagrindinių komponenčių analizę.

Stereotaksinių metodų ir dozės-tūrio metrikų palyginimą apsunkino skirtingi taikomi klinikiniai kriterijai, atsiskleidžiantys griežtesni pasitelkiant magnetinio rezonanso valdomos adaptyviosios radioterapijos (MRgART) strategiją. Tačiau analizė parodė, kad didesnė krūtinės ląstos dozė buvo reikšmingai susijusi su padidėjusia maksimalia planuojamo taikinio tūrio

(PTV) doze ($p = 0.007$), o tai rodo, kad sumažinus krūtinės ląstos klinikinius apribojimus galima labiau didinti dozę taikinio tūrio ribose. Maksimali krūtinės ląstos dozė taip pat parodė teigiamą ryšį su PTV $D_{98\%}$ aprėptimi, o tai rodo galimą kompromisą tarp pagerėjusio taikinio aprėpties ir padidėjusio krūtinės ląstos apšvitinimo. Priešingai, lung-GTV parodė reikšmingą neigiamą ryšį ($p = 0.044$) su maksimalia PTV doze, nurodantį griežtesnį plaučių dozės apribojimą, kuris gali suvaržyti pasiekiamą taikinio karštosios zonos intensyvumą. Stereotaksinis MRgART metodas, kuris statistinio modeliavimo tyrime pasiekė 24.19 išplėtimo vertę ties 10 mm parašte – daugiau nei dvigubai didesnę nei 5 mm parašte – gali būti laikomas jautriausiu ribos išplėtimo metodu.

Šiame tyrime pabrėžiama, kad judesių valdymo strategijos, įskaitant 4D-KT, kvėpavimo sinchronizavimą ir MRT valdomą adaptyviąją radioterapiją, yra labai svarbios siekiant sumažinti judesių neapibrėžtumą bei plaučių apšvitos ribas, padidinant dozimetrinį tikslumą, kadangi kvėpavimo judesiai turi didelę įtaką plaučių spinduliuotės planavimui. Be to, griežtesnis plaučių saugojimas riboja dozės didinimą taikinio tūrio ribose, o geresnis taikinio padengimas buvo susijęs su didesne krūtinės ląstos doze. Nepaisant to, remiantis statistiniu modeliavimu, mažesni taikinio tūriai parodė didesnį santykinį geometrinį augimą, kuris gali būti tiesiogiai susijęs su augančia netoliese esančio sveiko plaučių audinio apšvita.

Contents

List of tables

List of figures

List of abbreviations and terms

3D-CT – Three-Dimensional Computed Tomography

4D-CBCT – Four-Dimensional Cone Beam Computed Tomography

4D-CT – Four-Dimensional Computed Tomography

BED – Biologically Effective Dose

CI – Conformity Index

CTV – Clinical Target Volume

ED – Electron Density

EQD2 – Equivalent Dose in 2 Gy fractions

ERE – Electron Return Effect

FFF – Flattening Filter-Free

Fx – Fraction(s)

GTV – Gross Tumor Volume

HU – Hounsfield Units

IGRT – Image-Guided Radiation Therapy

IMRT – Intensity-Modulated Radiation Therapy

ITV – Internal Target Volume

LINAC – Linear Accelerator

LS-ERE – Lateral Scattered Electron Return Effect

MRgART – Magnetic Resonance-guided Adaptive Radiotherapy

MU – Monitor Unit

MV-CBCT – Megavoltage Cone Beam Computed Tomography

OAR – Organ-at-Risk

PTV – Planning Target Volume

SBRT – Stereotactic Body Radiotherapy

VMAT – Volumetric Modulated Arc Therapy

Introduction

Thoracic lung cancer, one of the most common cancers worldwide, accounts for over 25% of all cancer-related deaths, underscoring the disease's significance regardless of gender [14]. In recent years, stereotactic body radiation therapy (SBRT), which allows the delivery of highly conformal ablative radiation doses, achieving outstanding local tumor control and favorable clinical outcomes, has emerged as a recognized treatment option for patients with early-stage non-small cell lung cancer (NSCLC), especially for those who are medically inoperable [30].

Despite the clinical efficacy of the stereotactic approach and motion management strategies that enhance target visualization and reduce motion uncertainty during treatment delivery, tumor coverage and healthy tissue irradiation may be greatly impacted by even minuscule variations between the Gross Tumor Volume (GTV) and Planning Target Volume (PTV) margins, which may raise the risk of toxicity.

The possibility of real-time motion correction during ablative radiotherapy using magnetic resonance imaging of the target should outperform motion compensation strategies with current potential for margin reduction, tumor tracking, and plan adaptation. Even though lung SBRT has been extensively studied, limited research has focused on the dosimetric consequences of planning target volume distinction across magnetic resonance adaptive and four-dimensional computed tomography stereotactic strategies, particularly regarding the relationship between PTV coverage, hotspot intensity, and clinical dose limitations. Therefore, this project is focused on a retrospective quantitative dosimetric study based on comparative and statistical analysis of different lung planning methods.

The objective of this study is to differentiate the planned target volume and assess its dosimetric influence on target coverage and organ-at-risk sparing across different lung SBRT strategies.

Purpose. To evaluate and compare the structures of the planned target volume across lung radiotherapy methods implemented with different radiotherapy equipment, to determine their impact on clinical outcomes.

Work tasks:

1. To review scientific research on lung stereotactic body radiotherapy, focusing on treatment planning principles in thoracic radiotherapy.
2. To assess and compare the dosimetric characteristics of lung stereotactic radiotherapy strategies.
3. To analyze the differences in the planning target volume between conventional and stereotactic radiotherapy methods by developing statistical modulation.

Research methods: scientific literature analysis, quantitative statistical analysis of lung radiotherapy plans.

1. Literature review

1.1. Current lung cancer radiation therapy strategies

One of the most lethal malignancies worldwide is lung cancer [40]. It remains a noteworthy public health issue despite improvements in detection and treatment opportunities. Nonetheless, in both curative and palliative situations, radiotherapy is an essential part of the management of lung cancer. It is used as a main treatment or in conjunction with surgery, chemotherapy, and immunotherapy [40].

For patients with lung cancer who are not proper candidates for surgery, one of the primary therapeutic options is conventional radiation therapy. To reach the recommended total treatment dose, conventional fractionated radiation doses (usually 1.8–2 Gy per fraction) are delivered over a few weeks [34]. For larger tumors that have locally progressed or are situated near important organs such as the esophagus, central airways, or major blood vessels, this fractionated approach is fundamental. While progressively eliminating tumor cells, it permits the surrounding healthy tissues to repair radiation damage between therapy sessions. Radiotherapy methods, such as Intensity-Modulated Radiotherapy (IMRT) and Three-Dimensional Conformal Radiotherapy (3D-CRT), have greatly enhanced dose conformity and decreased radiation exposure to adjacent tissues at risk [34]. Additionally, the main tumor and the afflicted lymph nodes are usually treated with conventional fractionated radiotherapy, which is frequently coupled with chemotherapy. Taking into account that the lower dose per fraction reduces the risk of target localization errors and of severe toxicity, this type of radiation treatment may be more suitable in situations where tumor mobility cannot be sufficiently controlled or monitored [34].

Stereotactic Body Radiation Therapy (SBRT), often called Stereotactic Ablative Radiotherapy (SABR), is one of the most significant technological advancements in contemporary thoracic radiotherapy. It is an extremely accurate therapy method that administers high radiation doses to a specific tumor target in a few treatment sessions, known as fractions. To target the tumor precisely, this method uses highly conformal dose delivery, motion management techniques, and advanced imaging capabilities [46]. SBRT enables the delivery of a much greater biologically effective dose to the tumor while protecting nearby healthy tissues when compared with conventional radiation therapy. However, this treatment approach also has several limitations that are better managed with conventional radiotherapy. SBRT radiation treatment is typically not used for tumors that are within two centimeters of the proximal bronchial tree due to the significant risk of toxic outcomes. According to the guidelines for stereotactic radiation therapy by Csiki et al. [12], only lung lesions smaller than 5 cm should be treated. Additional contraindications to the use of stereotactic radiation therapy include susceptible target regions, multiple small-scale lesions, or even large lesions, according to Khan et al. [31]. These conditions limit the use of the treatment due to possible intolerable toxicity to healthy tissue.

1.2. Biological effect of lung radiation therapy

The assigned total dose, fractionation schedule, irradiated target volume, and the radiosensitivity of the surrounding healthy organs and tumor tissue all significantly impact the biological consequences of radiotherapy in cancer treatment. Dose conformity and normal tissue sparing have improved due to advances in treatment delivery methods. Nevertheless, maximizing therapeutic efficacy and lowering the risk of radiation-induced complications requires an understanding of the biological effects of various fractionation regimens and dosage limitations.

1.2.1. Regimes for dosage and fractionation

The recommended treatment dosage and fractionation for lung malignancies are greatly affected by tumor position, stage of disease, clinical objective, and the patient's ability to conform to the respiratory movement restriction technique during treatment. Modern techniques such as Volumetric Modulated Arc Therapy (VMAT) and IMRT offer improved conformity and sparing of organs at risk, which can be beneficial for both conventional and hypofractionated treatment regimens. For locally progressed, inoperable non-small cell lung cancer treated along with chemoradiation, the prevalent curative treatment is still delivered in 30 or 33 fractions, respectively, in 60–66 Gy (in roughly six weeks) [55]. Moderate hypofractionation may also be used when chemotherapy is not feasible, or treatment must be abridged; a typical regimen consists of 55 Gy in 20 fractions (treatment lasts a month) [55].

One of the most widely used radiation treatment delivery techniques for SBRT, the standard for early-stage control, is VMAT. It can deliver high radiation doses to a concentrated tumor with the ability to circumvent the aftermath of surgical difficulties. According to Chua et al. [9], treatment is usually administered in hypofractionated sets of three to five fractions of 10–15 Gy each, every other day. In contrast, lung tumors in the periphery could be treated with 54 Gy in three portions (in half a month) [8]. However, proven regimens for treating central lung malignancies include 50 Gy, 60 Gy, and 70 Gy, respectively, in 5, 8, and 10 fractions, to minimize toxicity (administered over 2 weeks, every second to third day) [4]. This is due to the greater risk of proximal bronchial structures.

Another important consideration is the opportunity for palliative radiation treatment. Minuscule radiotherapy course schedules, when 20 Gy (five fractions per week), 17 Gy (two fractions in eight days), or 10 Gy (single-fraction treatment), may be used for rapid symptom relief in progressed or metastatic tumor treatment conditions, according to guidelines from The Royal College of Radiologists (RCR) [55]. For patients with improved performance status or those seeking more long-term management, there are intermediate treatment schedules that take about half a month; during this time, the dose is delivered in 30 Gy (10 fractions), 36 Gy (12 fractions), or 39 Gy (13 fractions).

1.2.2. Guidelines on clinical limitations for lung tumor radiation treatment

Clinical limitations are essential to radiotherapy because they preserve the balance between treating the tumor effectively and protecting healthy tissue. Limitations help to reduce the risks of severe, possibly permanent or fatal, effects from ionizing radiation. Unfortunately, radiation dosage tolerance is influenced by the overall dose, fraction size, treatment purpose (palliative or curative), and patient life expectancy.

Despite being administered at a greater dose per fraction and with a fraction number three times lower than the curative regimen, palliative case therapy has more liberal limitations (Table 1) than conventional fractionation. However, due to the two-fold lower total dose of the treatment and the primary focus on comfort rather than long-term durability, the number of organs at risk (such as the lung-GTV, spinal canal, and brachial plexus) for palliative cases may be lower than in conventional treatment. The constraint of the lung-GTV makes treatment planning easier and faster, and enables a more precise evaluation of lung function exposed to radiation.

Table 1. Conventional and curative radiation therapies' clinical limitations (Barsky et al., 2020, Bisello et al., 2022)

Anatomical structure	Conventional fractionation (from 1.8 Gy to 2 Gy)	Palliative fractionation (3 -4 Gy)
Spinal cord	D_{max} < 45–50 Gy	D_{max} < 10-50 Gy
Spinal canal	D0.1cc < 45-50 Gy	-
Esophagus	D_{mean} ≤ 34 Gy; V_{35Gy} < 50%	D_{max} < 12-40 Gy
Lung-GTV	D_{mean} ≤ 18-20 Gy; V20Gy ≤ 35%	-
Lung-ITV	-	D_{mean} < 5.5 -10 Gy
Brachial Plexus	D_{max}0.1cc < 60-65 Gy	-
Heart	D_{mean} < 26–30 Gy; V30 ≤ 45Gy (V30Gy ≤ 30%)	D_{mean} < 20 Gy
Liver	V30 ≤ 40%	-

In SBRT, dose constraints are more stringent and typically defined over small volumes (e.g., D0.035cc), compared to conventional fractionation (60 Gy / 30 fractions) or even palliative regimens, according to the IBA Dosimetry established guidelines [27] (Table 2). Additionally, the inverse relationship is highlighted by SBRT dose-constraint guidelines: as the number of fractions increases, the dose per fraction decreases, allowing higher total dose limits for organs at risk while maintaining the same biological effect.

Table 2. SBRT radiation treatment clinical limitations (IBA Dosimetry, 2021)

Anatomical structure	Constraint	Number of fractions (fx)			
		3	4	5	8
Spinal canal	D_{max}(0.1cc) D_{max}(≤0.035cc)	< 21.9 Gy < 22.5 Gy	- < 25.6 Gy	< 30 Gy < 28 Gy	< 32 Gy -
Esophagus	D_{max}(≤0.035cc) D<5cc	< 32.4 Gy < 27.9 Gy	< 35.6 Gy < 30.4 Gy	< 38 Gy < 32.5 Gy	- -
Lung-GTV	D10% ≤ 20Gy D_{mean}	< 10-15% < 8 Gy	< 15% ≤ 6 Gy	< 10-15% < 8 Gy	< 10% -
Brachial Plexus	D_{max}(≤0.035cc) D_{max}(0.5cc)	< 26 Gy < 26 Gy	< 29.6 Gy -	< 32.5 Gy < 29 Gy	< 39.2 Gy < 38 Gy
Heart	D_{max}(≤0.035cc) D_{max}(0.5cc)	< 30 Gy (10 Gy/fx) < 26 Gy	< 34 Gy -	< 38 Gy (7.6 Gy/fx) < 29 Gy	<40 Gy < 60 Gy
Chest wall	D_{max}(≤0.035cc) D_{max}(0.5cc)	< 45 Gy < 40 Gy	< 54 Gy <43 Gy	< 57 Gy -	< 63 Gy < 39 Gy

In addition to healthy tissue dosage limitations, Planning Target Volume (PTV) and Clinical Target Volume (CTV) constraints determine the tumor dose to ensure tumor control and therapeutic effectiveness. Aslan & Aksozen [2] note that the objective of treatment planning is to ensure that at least 95% of PTV and CTV coverage would be received by 95% of the prescribed PTV dose (i.e., V95% ≥ 95%) and 98% of CTV dose (i.e., V98% ≥ 95%). However, the PTV must get at least 90–92% of the recommended dose (i.e., D95% > 90–92%) for palliative care [3]. The maximum dose guidelines for lungs are more flexible than for other organs because lung tissue has low density, so dosage calculations and adjustments often create hotspots within the PTV. Therefore, instead of less than 110% of the recommended dosage guideline [59], the lung radiotherapy treatment plans should not exceed 120–125% of the prescription dose [7].

1.2.3. Evaluation of biologically effective dose

Distinct fractionation regimes and total dosages are used in the conception of radiation therapy plans, depending on the magnitude of the tumor, severity, and the patient's status. In order to compare their biological impact on tissues and organs unaffected by the malignancy and cancerous growth, the Linear–Quadratic (LQ) model enables the determination of Equivalent Dose in 2-Gy fractions (EQD2) (2 Gy fractionations are typical doses in conventional radiotherapy for curative reasons) and Biologically Effective Dose (BED).

The amount of fractions and the recommended dosage for each fraction are the main factors in the BED estimation. This pair of variables determines the treatment's overall dosage. The ratio of alpha-beta, which describes how radiation destructs cells, varies between early and late-responding healthy tissue and tumor lesions: α/β = 3 Gy and α/β = 10 Gy, respectively.

Thus, an arithmetical expression for the BED formula and the effective dose may be estimated [17]:

$$\mathrm{BED} = \mathrm{D}\left[1 + \frac{d}{\alpha/\beta}\right]; \quad (1)$$

$$\mathrm{EQD2} = \frac{BED}{1+\frac{2}{\alpha/\beta}}; \quad (2)$$

when D - total dose of radiation, d - dose per fraction.

To illustrate the pivotal biological effects of lung radiotherapy on cancerous growth and normal tissues, the BED and EQD2 values may be calculated using the formulas above and applied to the aforementioned conventional, palliative, and SBRT treatments. Table 3 lists the outcomes.

Table 3. Radiobiological dose metrics are calculated based on the total dose and the fractionation regimen

Regimen	**BED_{10} (Gy)**	**$EQD2_{10}$ (Gy)**	**BED_3 (Gy)**	**$EQD2_3$ (Gy)**
Conventional 60 Gy / 30 fx (2 Gy)	72.00	60.00	100.00	60.00
55 Gy / 20 fx (2.75 Gy)	70.13	58.44	105.42	63.25
Palliative 20 Gy / 5 fx (4 Gy)	28.00	23.30	46.70	28.00
17 Gy / 2 fx (8.5 Gy)	33.50	27.90	72.90	47.50
10 Gy / 1 fx (10 Gy)	20.00	16.70	43.30	26.00
30 Gy / 10 fx (3 Gy)	39.00	32.50	60.00	36.00
36 Gy / 12 fx (3 Gy)	46.80	39.00	72.00	43.20
39 Gy / 13 fx (3 Gy)	50.70	42.25	78.00	46.80
SBRT 54 Gy / 3 fx (18 Gy)	151.20	126.00	378.00	226.80
50 Gy / 5 fx (10 Gy)	100.00	83.33	216.67	130.00
60 Gy / 8 fx (7.5 Gy)	105.00	87.50	210.00	126.00
70 Gy /10 fx (7.0 Gy)	119.00	99.17	233.33	140.00

Compiled by the author based on radiotherapy regimes used from scientific sources [55,56,4].

There are significant variations in value between BED and effective dose across treatment types and schedules, as shown in Table 1.

With EQD2 results of 17–42 Gy and BED_{10} values of 20-50 Gy, palliative treatment options offer comparatively modest tumor-effective doses. Such palliative regimens prioritize symptom alleviation and ease of treatment. Their poor biological ability is more consistent with improving conditions of life than with sustained tumor supervision. Even the most sophisticated palliative treatment options, such as 36 Gy or 39 Gy, achieve BED_{10} values of only up to 51 Gy, which is

still below the curative threshold, concluding radiotherapy regimens presented in the literature [55]. Nevertheless, Chow et al. [8] claim that treatment regimens over 35 Gy of BED_{10} are related to longer survival and a greater chance of symptom suppression.

On the other hand, curative, sort-of-conventional regimens provide far higher biological doses and attain BED_{10} values of roughly 70 Gy, which may be useful in locally progressed non-small cell lung cancer. BED_3 values around 100 Gy, however, indicate that these schedules also affect late-responding tissues more, indicating a higher chance of late toxicity in tissues and organs that are not harmed.

The most noticeable differences are in the SBRT regimen. The biological dose of conventional treatment is significantly lower than extremely high BED_{10} values (between 100 and 150 Gy). This outcome enables very high tumor biological doses to achieve remarkable local management rates [12]. However, SBRT produces extremely high BED_3 values (over 200–300 Gy) when given close to important structures, highlighting the potential for severe toxicity.

It can be assumed that BED values below 50 Gy do not significantly restrict tumor growth, based on the calculated tumor BED. Better local control and clinically considerable tumor inhibition, however, require a higher tumor BED result of 70 Gy or more. Furthermore, because even BED_3 can be greatly enhanced by a petite increase in dose per fraction, each organ has its own clinical constraint (sensibility to ionizing radiation), exceeding which can result in radiation-influenced issues.

1.3. Linear accelerator physics

The physical characteristics and technological capabilities of radiation delivery systems significantly affect the efficacy and safety of contemporary lung radiotherapy. The primary device used in external beam radiation therapy is the linear accelerator, which produces high-energy photon beams that minimize radiation to nearby healthy tissues while delivering conformal dose distributions to tumor targets. The accuracy of thoracic radiotherapy has been greatly enhanced by ongoing technological advances in image guidance, beam modulation, motion management, and adaptive treatment planning. Therefore, assessing the clinical use, dosimetric benefits, and limitations of conventional and magnetic resonance-guided linear accelerators in the treatment of lung cancer requires an understanding of their basic principles.

1.3.1. Properties of a conventional linear accelerator

Lung radiotherapy is delivered using a Linear Accelerator (LINAC), which generates therapeutic radiation through electromagnetic processes. The LINAC system accelerates electrons to high velocity using radio-frequency electromagnetic fields within a waveguide [50]. These electrons achieve energies ranging from kiloelectronvolts to megaelectronvolts. When these high-energy electrons collide with a high nuclear charge number target, generally tungsten, they undergo rapid deceleration, producing a spectrum of bremsstrahlung photons suitable for clinical application. This process generates a high-energy photon beam capable of penetrating deep

into biological tissues while preferentially depositing dose within the tumor volume rather than in superficial structures [50].

Precise beam shaping and accurate dose conformity to the tumor target are fundamental requirements for effective radiotherapy delivery. These characteristics are determined primarily by the beam collimation system, particularly the design and performance of the Multileaf Collimator (MLC). High spatial resolution of beam shaping is essential in stereotactic body radiotherapy to achieve steep dose gradients and optimal target coverage. Previous studies have demonstrated that, for accurate SBRT delivery, the width of MLC leaves should not exceed 1 cm [50]. In fact, the leaf widths of 5 mm or less are preferable to ensure precise beam modulation and high-quality dose distribution to the target volume [50].

1.3.1.1. Image-guided radiotherapy integration

To further improve geometric precision and reduce uncertainties arising from patient setup, anatomical changes, and tumor variations, a few established techniques (e.g., MV, kV, and optical) can help ensure patient positioning before radiation delivery.

Image-guided Radiotherapy (IGRT) modality of kilovoltage (kV) Cone-Beam CT (CBCT) imaging

To track and capture any unclear target derangements caused by the patient's inevitable movements, the three-dimensional cone-beam CT method shows the patient's anatomy before each fraction. According to Gutiérrez et al. [21], however, the phase of breathing projections are averaged to produce a single three-dimensional scan for lung movement tracing, which can lead to artifacts or hazy zones of interest that provide false information about the tumor's location.

Nonetheless, 4D-CT provides better tracking of respiratory movements, which is extremely important when treating lung malignancies. According to Gutiérrez et al. [21], this approach reduces inter-observer variability in patient positioning by keeping the margins surrounding the tumor target narrow and providing additional information on the target’s interfractional placement.

IGRT modality of megavoltage (MV) imaging

According to Hwang et al. [26], MV imaging is performed using the same radiation source as treatment. The primary advantage of this technique over kV imaging is the decrease in geometrical errors. Electronic portal imaging equipment, fan-beam MV-CT, MV-CBCT, and the provision of three-dimensional images prior to treatment can all be used to obtain images of MV as a quick, easy way to modify dosimetry and confirm modulated delivery [21].

IGRT modality of optical imaging

According to Gutiérrez et al. [21], a system of respiratory gating can administer radiation at specific stages of the breathing cycle. Optical imaging is primarily useful for patient monitoring during treatment and for evaluating patient position before treatment.

However, tumor mobility can be observed using only 4D-CT with an infrared camera, and optical and megavoltage imaging techniques are primarily used for patient positioning adjustments. The special block of infrared marker, situated on the patient's chest, shows breathing activity, which is followed by the camera equipment as it scans the patient's surface. Moreover, according to Ghani & Ng [18], a transducer of pressure, which measures constriction from the dilation (breathing in) and contraction (breathing out) of the chest, might be utilized to track down the breathing volatility of movement with the chest belt. It is possible to derive intrinsic respiration patterns from 4D-CT images acquired in simulation, which can then be matched to known tumor therapy scenarios.

1.3.2. Properties of magnetic resonance linear accelerator

Radiation therapy delivery with Magnetic Resonance Imaging (MRI)-guided linear accelerators demonstrates a relevant innovation in oncology treatment. This combination allows improved image-guidance not only to ensure and verify patient setup before treatment, but also throughout treatment delivery. MRI imaging greatly enhances image-guidance, especially for soft-tissue targets that are challenging to locate with X-ray-based imaging due to lower soft-tissue contrast, scattering artifacts, or inadequate differentiation of target density [41].

Applying a magnetic field, which is either 0.35 T or stronger (e.g., 1.5 T), provides better resolution and image quality, and radiofrequency pulses that excite hydrogen protons in tissue and produce detailed data based on their relaxation properties [41]. The MRI component continually creates real-time images. This significant data is processed to rebuild images of the tumor and nearby biological structures without additional ionizing radiation. To generate photons suitable for therapeutic irradiation, the integrated LINAC component operates similarly to a conventional LINAC system, with MRI guidance added to improve treatment targeting.

1.3.2.1. Occurring challenges with the magnetic field

The beam properties, dose distribution, and tumor-target focusing are greatly influenced by physical interplay. Charged particles, such as secondary electrons created by photon interactions within the patient, interact with the static magnetic field. These electrons in an MRI-LINAC move along spiral pathways rather than linear trajectories due to the Lorentz force. However, the Electron Return Effect (ERE) can occur due to pushed-back secondary electrons passing through a magnetic field toward the tissue surface at density boundaries [57]. Because electrons move along paths forced by the magnetic field, the ERE can result in hot blotches at soft-tissue–air interfaces (e.g., in air-filled organs such as the lungs), local dose enlargement, or changes in the beam penumbra and impact the overall electron scatter equilibrium [57].

Moreover, the return effect of Laterally Scattered Electrons (LS-ERE) can lead to dose differences across distinct anatomical interfaces, resulting in hotspots near the ridges of the

radiation beam due to the lateral-scattered electrons coiling back into the interface of nearby low-density material [53]. This type of ERE pushes the dose closer to the body surface, which is directly associated with greater skin exposure [35,22]. As a result, this outcome produces a steeper dose gradient, making it difficult to plan small targets, especially in low-density, heterogeneous tissues. These ERE effects highlight the importance of thorough modeling in MRI-LINAC treatment planning.

1.3.2.2. Adaptive MRI-guided radiotherapy

By enabling radiation treatment plans to be adjusted over the course of treatment in response to anatomical changes and tumor target position variability, Adaptive Radiotherapy (ART) is a major advancement in SBRT for lung cancer. This conception differs from traditional radiation treatment, which uses a single radiotherapy plan created during simulation for each fraction. This planning method can result in incomplete target dose coverage due to interfractional fluctuations in tumor extent, structure, and motility, as well as in the placement of nearby healthy organs [12].

MR-guided Adaptive Radiotherapy (MRgART) enables daily image acquisition right before each session, based on the patient's current anatomy. This nonionizing imaging during treatment enables clinicians to reassess and, if needed, re-optimize the treatment strategy. In comparison to non-adaptive plans, dosimetric studies have demonstrated that the adaptive MR-guided technique can increase both PTV coverage and sparing of Organ-at-Risk (OAR). The study by Regnery et al. [45] accounted for the complex locations of lung tumors (not only non-peripheral but also centrally located), which may overlap with intact tissues and organs, when planning radiotherapy. Plan adaptation effectively corrected poor target coverage in the majority of cases; whereas 86% of predicted non-adaptive plans would have resulted in inadequate PTV coverage, this proportion decreased to only 13% following adaptive replanning, highlighting the clinical value of adaptive radiotherapy in ensuring consistent target dose delivery [45]. This resulted in quantifiable increases in the biologically effective dose within target volumes and enhanced safety margins for sensitive tissues. These advantages were particularly apparent when the tumor showed considerable mobility, deformation, or was situated near important healthy structures [45]. However, according to Bryant et al. [7], in the majority of SBRT cases, the initial Gross Tumor Volume (GTV) contour stays stable during treatment.

Additionally, MRgART allows for both geometric and functional adaptation, whereby imaging biomarkers (such as MRI radiomics and intra-fraction motion measurements) can guide therapy optimization based on biological response patterns as well as anatomical structure. Recent trials and experiences demonstrate the viability, safety, and potential clinical benefit of adaptive MR-guided SBRT for lung tumors, despite certain implementation challenges, including the complexity of on-table planning, prolonged treatment times due to imaging and re-optimization, and the need for multidisciplinary coordination [44]. To provide individualized, motion-informed, and dose-optimized lung SBRT, MRgART is expected to become increasingly crucial as imaging technology and adaptive planning algorithms advance.

1.3.3. Significance of relative electron density

The quantity of electrons per unit volume of a material is described by the fundamental physical property known as Electron Density (ED). It is crucial not only to scattering but also to the absorption of X-rays, and is directly correlated with the density and nuclear charge number of the matter [47]. A tissue's X-ray attenuation characteristics are influenced by its electrical density. The energy scale of the X-ray photons at 120 kV maximizes the ability to distinguish between tissues (soft tissue, bone, and fat structures) with varying densities of electrons [47]. Additionally, the photoelectric effect and Compton scattering are necessarily involved in X-ray interactions with tissues, providing the basis for the observed differences in ED between anatomical structures [47].

In computed tomography, the radiodensity of tissues is quantified using the Hounsfield Unit (HU) scale. These units show the grade to which a material attenuates X-ray beams in comparison to reference materials, concretely air (-1000 HU) and water (0 HU). These values of HU can be determined by the following formula:

$$HU = \frac{\mu - \mu_{water}}{\mu_{water}} \times 1000; \qquad (3)$$

where μ is the tissue's linear attenuation coefficient, and μ_{water} is the water's attenuation coefficient.

The ED of tissues and HU values derived from computed tomography images are crucial for radiotherapy planning. A calibration curve (Fig. 1) relating Hounsfield Units (HU) to relative ED with respect to water is used for dose calculation [47].

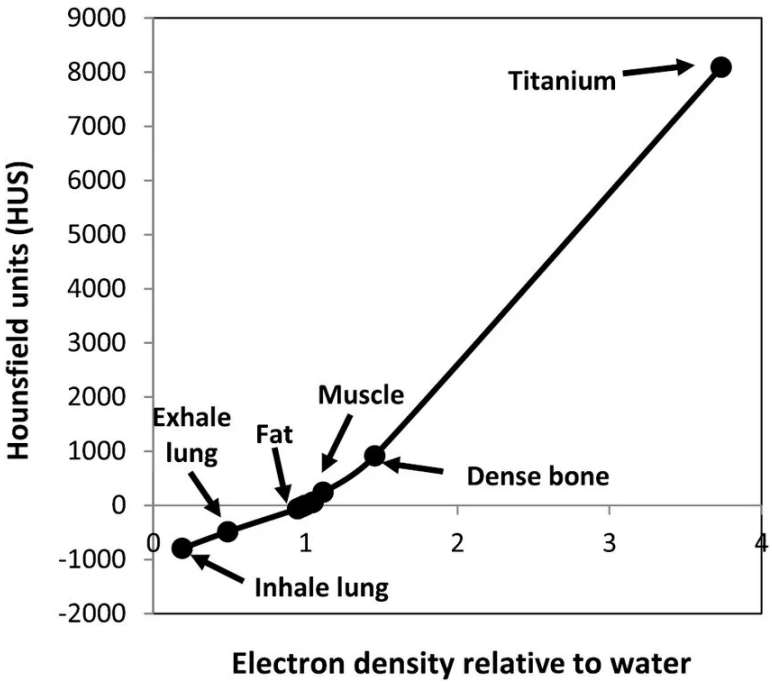

Fig. 1. Hounsfield unit and relative electron density calibration curve (Hsu et al., 2018)

A map based on the patient's electron density is produced once the treatment planning system has converted all HU values to ED. The treatment planning system then computes how radiation will interrelate and be absorbed by various tissues using this density map [47]. The system modifies the distribution of the dosage in accordance with the fact that greater ED tissues, such as bone, will weaken the beam more than lower ED matter, such as lungs.

Magnetic resonance imaging does not provide information on electron density or photon attenuation, unlike CT. Proton density and tissue relaxation characteristics, which are unrelated to RED, determine the strength of the MRI signal. Therefore, the indirect calculation method must be applied to estimate RED to alleviate the burden of MRI-based radiation planning. The creation of synthetic CT (sCT) images from MRI is the most widely used approach. These sCT datasets provide tissues' pseudo-HU values, which are further transformed into RED using standard calibration curves. Therefore, to ensure precise anatomical congruence between electron-density data from CT and the improved soft-tissue imaging provided by MRI, both CT and MRI datasets are acquired during simulation in the treatment position [7]. The planning CT is deformably registered to the MRI to impart ED information for dosage computation, while the simulation MRI remains the main dataset for target delineation and motion management.

However, there are exceptions to lung planning that allow for more optimal plan preparation by manually assigning the appropriate PTV electron density and creating auxiliary structures as needed. Grace E. A. Healthy et al. [23] study highlights that overriding the planning target volume with a relative electron density of 0.650 produced the best balance between lung tumor conformity, homogeneity, and target coverage in lung SBRT. This result is an effective density that takes into consideration motion-induced averaging effects and the combination of the tumor and adjacent low-density lung tissue within the PTV. In contrast, lower electron densities (e.g., 0.475) or greater densities (e.g., 1.0) resulted, respectively, in overestimation (less attenuation assumed) or underestimation of the prescribed dose [23]. Unfortunately, this value has a limitation: it applies only to targets with a diameter of 2.2-3 cm.

Also, to ensure accurate dose calculation between tissue and air structures for MRI-LINAC-based treatment, a ring structure called "Lungs 1.5 cm" can be created around the GTV. It would guarantee the creation of a larger ED area in the lung. This additional structure creation highlights that clinical optimization often requires these unique shell designs to avoid cold spots that arise when the magnetic field pushes electrons into the surrounding healthy lung, away from the target boundary [11].

1.3.4. Dosimetric precision

The dosimetric precision of a linear accelerator is a fundamental determinant of clinical outcomes, particularly in hypofractionated regimens and stereotactic body radiotherapy, where small field sizes and steep dose gradients demand exceptionally high accuracy. This precision is achieved through meticulous machine commissioning, including comprehensive measurements of depth-dose curves and beam profiles, combined with continuous quality-assurance programs that ensure long-term mechanical and dosimetric stability. When properly

commissioned and validated, in line with the monthly recommendation from International Atomic Energy Agency (IAEA) TRS-398 [28], modern LINAC systems can maintain reproducible output, typically within ±2% variability. An additional advantage of LINAC-based delivery is the ability to modulate beam intensity across the field, creating non-uniform dose distributions in which the tumor receives the highest dose while the dose progressively decreases toward the target margins, effectively sparing surrounding healthy tissue. Daily laser localization and IGRT registration accuracy should be typically kept within 1–2 mm or less for stereotactic treatments (for conventional treatments, this parameter should not exceed 3 mm), and mechanical radiation isocenter precision should be 1–1.5 mm or less for SRS/SBRT (conventional radiotherapy – ≤ 2 mm) [10].

1.3.5. Algorithm for dose calculation

In lung radiotherapy, the Acuros XB algorithm is widely used for dose determination due to its advanced physics-based modeling capabilities. This calculation algorithm is founded on the Linear Boltzmann Transport Equation (LBTE), which describes the fundamental interactions between ionizing radiation and matter, including scattering, absorption, and charged-particle transport in complex geometries and heterogeneous media [16]. This theoretical framework enables the algorithm to accurately model radiation transport in anatomically complex environments characterized by varying tissue densities and compositions.

In the context of lung radiotherapy, Acuros XB accounts for the presence of multiple tissue types, including soft tissues, bone structures (spine, sternum, rib cage), and low-density air-filled lung regions, as well as conditions of charged-particle disequilibrium. This capability enables more precise estimation of dose deposition in anatomically challenging regions, particularly where photon beams traverse low-density lung tissue or air cavities, and in small-field irradiation scenarios typical of lung tumor treatments, where simplified algorithms are prone to significant dose-calculation errors.

Multiple studies have demonstrated that Acuros XB achieves dose-calculation precision within 3% of Monte Carlo simulations in lung tissue and heterogeneous phantom models, highlighting its reliability in clinically complex environments [16]. This accuracy is achieved because Acuros XB does not rely on water-based convolution kernels or simple density-scaling approximations; instead, it explicitly models particle transport in heterogeneous media.

Furthermore, Monte Carlo-based dose calculation (e.g., Monaco) for MRI-LINAC, where electron transport physics is further complicated by magnetic field effects, also improves accuracy in heterogeneous lung tissue in clinical practice and facilitates plan modification and verification procedures [48]. To further improve quality assurance in adaptive workflows, independent Monte Carlo dose-check engines are increasingly used to verify primary dose estimates prior to treatment approval.

In contrast, the Analytical Anisotropic Algorithm (AAA) is based on a convolution–superposition approach that scales precomputed scatter kernels in water according to tissue density [52].

Because AAA does not explicitly model electron transport in heterogeneous tissues, it exhibits reduced accuracy in low-density regions such as the lung, often underestimating attenuation and overestimating dose within lung tumor targets. Consequently, Acuros XB and Monte Carlo methods provide superior dosimetric performance for lung radiotherapy, particularly in regions characterized by strong tissue heterogeneity and steep dose gradients.

1.4. Planning aspects in lung tumor radiotherapy

Explicit delineation of the tumor and treatment dose administration is more difficult due to the lungs' constant motion, which is inevitably caused by both breathing and cardiac movement. Gutiérrez et al. [21] claim that computed tomography diagnostic images, typically obtained with a width of 2.5 mm per slice, are the first step in radiotherapy planning. These images are usually obtained with a contrast agent, which allows clear visualization of the tumor edges and their extent. The apparent tumor mass and affected lymph nodes are delineated by the gross tumor volume. Savanović et al. [49] claim that a single set of fixed images taken at any time throughout the respiration cycle might form this GTV planning region.

The clinical target volume, especially important in non-small cell lung tumor radiotherapy cases, encompasses the full extent of adjacent tissues in which cancer cells might have microscopically disseminated and cannot be seen on imaging or otherwise detected. This volume guarantees improved treatment efficacy and lowers the risk of cancer recurrence. Nevertheless, since early-stage cancerous growth seldom expands beyond the visible borders, CTV is typically regarded as equal to GTV in lung SBRT [20].

The PTV is obtained by enlarging the Internal Target Volume (ITV), which accounts for the target mobility path through unavoidable patient breathing and internal organ motion, or by adding a verge to the CTV to justify patient setup fallacies, biological structure motility, and machine-associated indeterminacy. The structure of the tumor target volume for radiotherapy is presented in Figure 2.

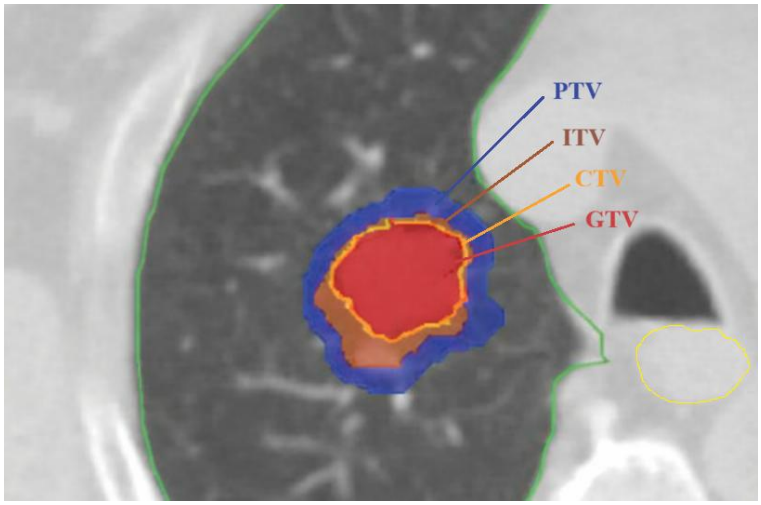

Fig. 2. Delineation of tumor target volume in the lungs (Savanović et al., 2021)

However, tumors up to about 4-5 cm in diameter show the best results with the SBRT method. Furthermore, moving and shifting tumor targets in the lungs may not be well distinguished by three-dimensional CT alone. Because it captures several stages of the respiratory cycle and allows evaluation of tumor internal mobility, four-dimensional CT is considered one of the greatest imaging strategies for SBRT.

This delineation of the target is often carried out during the patient's respiratory cycle, following simulation for radiotherapy using CT or MRI scans. For CT-based treatment, ten phases can be identified in these images, with the phase of utmost inspiration denoted by 50% and the phase of exhalation by 0%. Conversely, to guarantee proper tracking for MRgART delivery, a half-minute cine sequence is often acquired while the patient cycles between free-breathing and breath-holding techniques, which allows for defining the area of the tracking structure - gating envelope [7]. To assure proper dosimetric coverage, the PTV should entirely be enclosed by this boundary structure, created with a 0.3 cm margin from the PTV, according to Bryant et al. [7].

1.5. Tumor motion management methods

Unavoidable breathing motion poses a unique challenge for radiation delivery during treatment procedures. It can cause a tumor to change position by several millimeters or even centimeters, which could affect the accuracy of the dose and raise the possibility of irradiating healthy lung tissue. In order to account for or minimize tumor mobility during treatment planning and delivery, radiotherapy employs a few motion-management and tumor-tracking techniques.

1.5.1. Active breathing motion control possibilities

Respiratory gating technique

Radiation is only administered during a certain part of the breathing cycle when the tumor is in a stable and predictable location. However, when the tumor target shifts beyond these gating window boundaries, the radiation beam supply is halted. There are two alternatives to achieve this gating method: phase and amplitude.

According to Joe et al. [29], the phase-gating strategy entails administering radiation during a predetermined phase of the patient's breathing cycle, usually during the breathing-out stage. Nevertheless, this approach is highly susceptible to irregular breathing (unforeseen respiratory changes) (Fig. 3), which may halt the distribution of the dose until regular breathing is resumed. This approach may not be a particularly successful solution due to the pathway's specificity, which could lead to longer treatment times due to uncontrollable patient breathing artifacts [32].

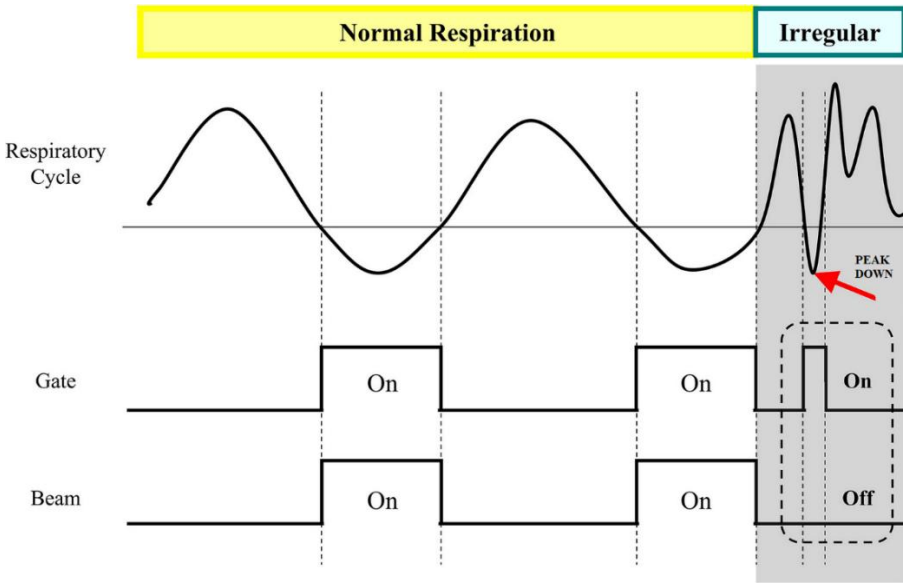

Fig. 3. Strategy of phase gating (atypical breathing rhythm affects the cutoff of treatment delivery) (Lee et al., 2019)

According to Meyers et al. [36], a "window of delivery" is selected during therapy that automatically activates when the cue is compatible within a predetermined range of amplitude. Otherwise, one of the other windows for treatment administration might be selected for the activation of the radiation treatment window when the target tumor is in an expiratory phase setting. Usual breathing can be included in a wide-ranging gating window, but when an abnormally large or atypical pattern of respiration appears during breath-in or breath-out, the radiation delivery would not be provided. Meyers et al. [36] claim that the treatment could only be accomplished during the breath-out phase, when the treatment delivery is on approximately half or only a third of the time during the radiation therapy; correspondingly, 30-70% and 40-60% of images of the phase would be helpful for ITV delineation and treatment arrangement, respectively (Fig. 4).

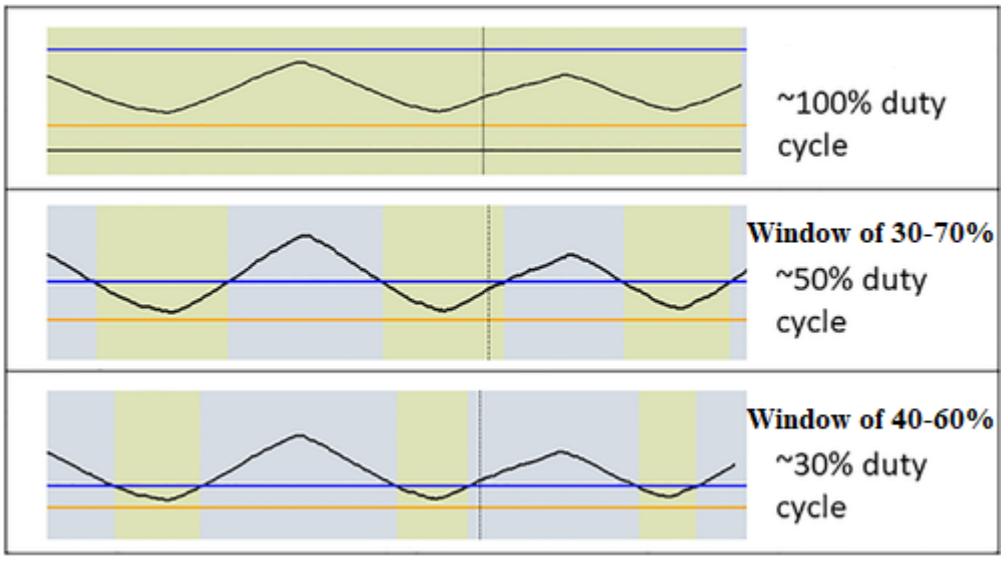

Fig. 4. Strategy of amplitude gating, where the boundary of orange and blue color indicate the window of gating, while green specifies delivery of radiation) (Meyers et al., 2022)

Prunaretty et al. [43] state that an infrared camera is used to follow valid movement, and the special reflective feature marker, which must be placed on the patient's chest area, justifies the relation of the tumor placement with the patient's breathing pattern. Nevertheless, this method has drawbacks and cannot be applied to patients who are unconscious or have impaired lung function.

Breath-hold technique

This type of breathing management control (Fig. 5) is commonly used in radiotherapy to minimize the effects of respiratory motion. When it is applied, tumor movement is temporarily suppressed, and therefore, the ITV can often be considered equivalent to the GTV. In such cases, target delineation is typically performed on three-dimensional images obtained from selected respiratory phases, most commonly at the end of breath-in or end of breath-out, derived from a dataset of four-dimensional computed tomography [51].

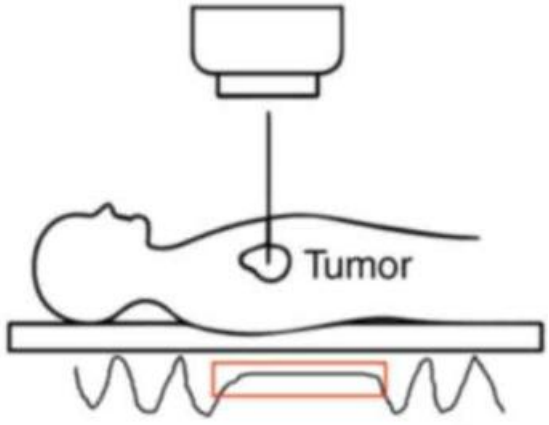

Fig. 5. Example of breath-in respiratory pattern during the breath-holding method (Shao et al., 2025)

During the inhalation stage, notable anatomical changes occur within the thoracic cavity; the lungs dilate, the diaphragm descends, and structures of the mediastinum become more separated [51]. A profound inhalation hold can be performed using an active respiratory control system, which temporarily obstructs airflow once a predefined lung volume is reached. Alternatively, voluntary breath-hold techniques can be used, where patients hold their breath following respiratory coaching and are observed using optical response systems or surface-tracking technologies to ensure consistent inhalation depth between treatment sessions [51].

Although deep inspiration breath-hold is less frequently used than respiratory gating in lung stereotactic body radiotherapy, it offers several advantages for motion management. Unlike gating, which repeatedly interrupts the radiation beam according to the respiratory cycle, this method allows radiation delivery during each breath-hold period. Treatment is typically administered over several repeated breath-hold cycles within a single fraction. Furthermore, deep inspiration increases lung volume, which can reduce the relative radiation dose delivered to the lungs for the same treated target volume [51].

1.5.2. Passive breathing motion control possibilities

Target tracking technique

One of the key advantages of tumor tracking systems in radiotherapy is their ability to monitor the tumor position continuously during treatment. This is often achieved using fiducial markers, small radiopaque markers that are placed inside or near the tumor, typically during a bronchoscopy procedure. These markers serve as reference points that allow clinicians to follow the tumor's movement throughout the treatment session.

According to Tanaka et al. [54], radiation delivery can be guided by tracking these markers as they move with the tumor. Treatment is performed when the markers enter a predefined spatial region known as the gating window or gating box, which is usually defined as a small three-dimensional volume. Additionally, target volume definition is commonly performed using the internal target volume concept. In this method, the tumor is contoured across several selected phases of the respiratory cycle, and these individual contours are combined to generate a single ITV that represents the entire scope of tumor motion [54]. This ensures that radiation would be administered solely when the target is within the planned treatment position.

Because the breathing cycle is not symmetrical, the exhalation phase tends to be longer and more stable than the inhalation. For this reason, radiation is commonly delivered at the end of exhalation, when the tumor position is more consistent and remains relatively stationary for a longer period of time. This improves treatment precision and allows a longer continuous radiation delivery window.

The position of the fiducial markers relative to the tumor can be monitored using X-ray imaging approaches such as cone-beam computed tomography, electromagnetic transponders, or through correlation models that relate external respiratory signals (surface monitoring) to internal tumor motion [51]. Continuous imaging ensures that the markers remain within the

predefined gating volume before radiation is initiated, thereby maintaining accurate targeting throughout the treatment.

The patient's erratic and fluctuating respiration during regular breathing is one of the challenges in radiation treatment planning that must be considered. The tumor's movement is greatly influenced by the patient's breathing frequency and inspiratory volume.

Free-breathing technique

This method allows patients to breathe normally during the radiotherapy procedure while radiation is administered to the tumor throughout the entire breathing cycle. Therefore, this technique could be devoted to patients who are unable to hold their breath or comprehend respiratory patterns. To account for tumor motion under these conditions, four-dimensional computed tomography is used during treatment planning. This imaging technique synchronizes respiratory signals with CT image acquisition, enabling clinicians to visualize how the tumor position changes over time during the breathing cycle. Generally, target delineation is achieved from ten breathing stages, with GTV limits determined at each stage [51]. An ITV margin is created by adding together all of the defined GTVs [51].

One method used to reduce target motion during free-breathing radiotherapy is known as abdominal compression (Fig. 6). This technique involves applying an external mechanical constraint, such as a belt or compression plate, to the upper abdomen in order to limit the amplitude of respiration [51]. This approach is particularly beneficial for patients who experience significant respiratory-induced tumor movement, especially in cases where tumors are located in the lower lobes of the lungs, as tumor displacement in this region is strongly influenced by diaphragmatic motion [51].

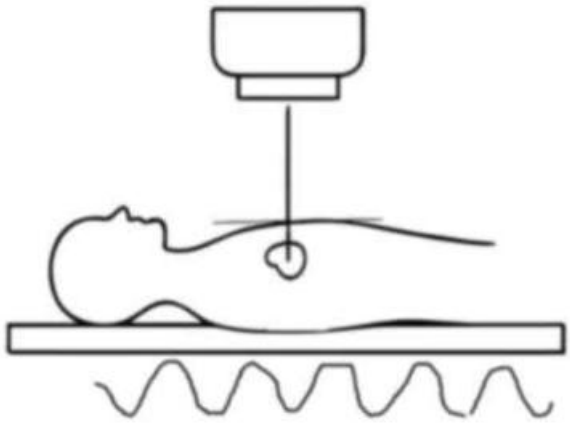

Fig. 6. Example of breathing patterns during the abdominal compression method (Shao et al., 2025)

However, because this approach requires larger treatment margins to compensate for tumor motion, it may lead to a higher radiation dose being delivered to the surrounding healthy tissues compared with other motion-management techniques. For this reason, its use has gradually decreased as more advanced strategies for managing respiratory motion have been developed.

1.5.3. MR-guided motion management abilities

Recent advancements in MR-guided radiotherapy systems have made it possible to visualize tumor motion during treatment directly. Despite the fact that traditional motion-management techniques are frequently based on CT imaging, which includes additional dose exposure, the dependence on external surrogates, and fiducial markers to enable solutions that can reduce target volume.

The treatment delivery system in MRI-guided adaptive radiotherapy uses image registration algorithms to continuously compare real MRI anatomy with the initial axial treatment planning dataset. Bryant et al. [7] state that obtaining sagittal and coronal template images from the daily volumetric MRI dataset is the first step in the tracking process. This visualization of tumor displacement in the anterior-posterior (coronal view of motion) and superior-inferior (sagittal view) directions, which predominate during thoracic respiration. Technology establishes spatial congruence between the intended target position and the anatomy observed during treatment by matching the template images to the planning MRI using mutual-information-based registration [7]. The GTV and an additional binary mask margin are then employed in cross-correlation methods to register incoming MRI frames to the template images [7]. Both the absolute and relative registration components are used to determine the overall observed target displacement.

Four-dimensional magnetic resonance imaging (4D-MRI)

This technique captures images of a tumor at different stages of the breathing cycle. These images can then be used to create either motion-averaged images or mid-position images [13]. The MRI signal potency is averaged over the whole breathing pattern to provide a motion-averaged image. However, this image capturing can provide vigorous blurring of the tumor target and restrict precision and obfuscate target borders [13]. Though mid-position images determine the average anatomical location without blurring artifacts, and allow establishing a more exact ITV (requires a longer reconstruction time).

4D-MRI allows one to assess the daily motion of the tumor and verify whether the planned treatment volume still covers the target accurately. The technique shows an advantage of PTV adjustment if the tumor moves beyond the originally planned volume and ensures that the tumor continues to receive the prescribed radiation dose and that the risk of under-treating the tumor is minimized [13].

Breath-Hold MRI

MR-guided breath-hold techniques are based on the same principle as breath-hold methods used in conventional radiotherapy. Nevertheless, this guiding method does not rely on external monitoring devices or require internally inserted fiducial markers to verify the tumor position. Instead, the tumor can be visualized directly on MRI images, allowing confirmation of its position during each breath-hold at the end of inhalation or the end of exhalation [13]. Without any supplementary radiation dose for target visualization, this method enables repeating breath-

hold scans until a stable and reproducible position is achieved. This feature is particularly helpful for tumors located close to important organs, such as central lung tumors, where even small positional changes may influence the radiation dose delivered to nearby structures [13].

Some MR-LINAC systems include automatic gating functionality, which pauses radiation delivery if the tumor moves outside the predefined breath-hold position, while other systems may require manual interruption of the beam when the tumor moves outside the acceptable position.

Cine-MRI

During this real-time imaging technique, the images are combined into a dynamic sequence that shows how the tumor and surrounding tissues move during respiration while radiation is being delivered. The cine-MRI modality can be useful for intra-fraction monitoring, meaning the tumor position can be checked throughout the entire treatment session [13].

Modern MRI sequences used in radiotherapy can acquire images at approximately 4–8 frames per second [13]. These images are usually obtained in selected two-dimensional planes that intersect the tumor or nearby critical organs, allowing continuous visualization of the treatment area. Continuous MRI monitoring also makes it possible to detect unexpected or irregular movements that may occur during treatment and pause treatment if necessary, helping ensure that radiation is delivered accurately to the intended target.

1.6. Planning target volume variability in lung radiotherapy

Ionizing radiation dedicated to the tumor target may also be administered to nearby tissues, despite radiotherapy being an advanced treatment modality. When tumor placement determination is disturbed due to respiratory movements, this could result in underdosage in subsequent fractions or inadvertent dose growth. To address these issues, the PTV volume is determined appropriately, taking into account not only the condition of the tumor being treated, but also the respiratory control method and the radiation therapy imaging method.

For the conventional treatment approach, based on 3D-CT, a 5 to 10 mm margin should normally be applied when everyday IGRT is employed, and internal target motion is taken into account to create a PTV verge; larger (about 10–20 mm) margins can be applied when IGRT or respiratory movement control is not used [19].

In contrast, SBRT, typically based on 4D-CT, relies on more accurate geometric and mobility management to deliver radiation with incredibly steep dose gradients. A verge of 3-5 mm should be applied to CTV to compensate for PTV coverage due to the possibility of tumor relocation during patient respiration and the foreseeability of tumor tracking when active or passive breathing control systems are utilized [43]. However, the scientific research by Trémolières et al. [58] found that a 0,5 cm margin to allow for PTV under the free-breathing SBRT approach does not always achieve desired target coverage results because of motion variability with each

treatment situation. Because of this, the idea of PTV planning is still debatable and could change based on how the free-breathing notion is applied.

In MR-guided radiotherapy, the size of the planning target volume margin depends largely on the motion-management strategy used during treatment. For example, Das et al. [13] reported that a PTV margin of approximately 3 mm was adequate to account for most geometric uncertainties when treating the lungs under breath-hold and gated respiratory conditions. However, Das et al. [13] also suggested that larger margins may be necessary in a non-gated or free-breathing approach, where respiratory motion introduces additional uncertainties. In these cases, the selection of the PTV margin depends on the anatomical site and clinical protocol, but typically ranges from approximately 3 mm to 5 mm (or even up to 10 mm).

2. Empirical part

This quantitative study is divided into three parts, two of which review both magnetic resonance and computed tomography-guided stereotactic radiotherapy methods of the lung, and a statistical modulation analysis that abstractly compares the influence of GTV and margin size on PTV outcome in both stereotactic and conventional radiotherapy. All selected lung radiotherapy plans were collected from X Healthcare Facility. The gathered data was analyzed statistically and visualized using RStudio software.

2.1. MRI-guided lung SBRT research methodology and methods

This part of the study evaluates five lung tumor cases planned for ablative radiotherapy using a 1.5 T Elekta Unity MR-Linac. Treatment plans were prepared for implementation using balanced Turbo Field Echo (bTFE) Fast cine MRI tracking in real time, with sagittal and coronal respiratory motion views. Each treatment case investigates a tumor in the right lung, placed in the periphery, except for the second case, in which the tumor is located in the central part of the lung. The lung treatment plans were planned with a 0.5 cm PTV margin from the CTV (or GTV), but the second treatment plan differed with a wider PTV margin, which reached 1 cm. The same dosimetric protocols were used for all stereotactic treatment plans with the MRI linear accelerator.

For dosimetric analysis, plans were created using a 7FFF photon beam with the Monaco 6.2.2.0 online treatment planning system, GPUMCD algorithm, which has 2% statistical uncertainty per calculation, and IMRT beam delivery method. IMRT sequencing properties involve a minimum area of segment 2 cm^3 and a width of 1 cm; the range of treatment monitor units (MU) per segment is from 4 to 110. This limited MU units per segment is an important planning parameter that must be considered to ensure the treatment plan is implemented within the maximum allowed MU / Segment (to avoid splitting into two treatment plans) and that the segment number is sufficient to circumvent obliterated beam fields. Verification of the plans was performed using the ArcCHECK phantom.

2.1.1. Clinical constraints for stereotactic MRgART plans

All lung treatment plans were designed according to the curative treatment approach. A total dose of 40 Gy administered in 5 fractions (8 Gy per fraction) was chosen for cases II-IV, and a total dose of 50 Gy / 5 fractions (10 Gy per fraction) was delivered for cases I and V.

Clinical limitations for organs at risk were chosen while taking the fractionation regimen into account, and PTV and GTV coverage limitations were adhered to (Table 4). Although there is significant variation between cases, the results show that all planning objectives were met within the specified tolerance levels. Nonetheless, the observed differences show how patient-specific anatomy and constraint prioritization affect the ultimate distribution of doses.

Table 4. Results of clinical constraints for the lung SBRT MRI-LINAC plans

Clinical constraints		I Case	II Case	III Case	IV Case	V Case
		Dose (Gy)				
PTV	CI ≥ 1 (-0.3)	0.70	0.86	0.70	0.70	0.70
	Dmax ≤ 60Gy (+2.5Gy)	54.35				52.63
	Dmax ≤ 48Gy (+2Gy)		45.52			
	Dmax ≤ 44Gy (+2Gy)			42.92	42.81	
	D99% ≥ 36Gy		38.10			
	D98% ≥ 47.75Gy (-2.5Gy)	49.16				49.23
	D98% ≥ 38Gy (-2Gy)			38.70	39.50	
	D95% ≥ 39.6Gy		39.61			
Chestwall	Dmax ≤ 57Gy	52.59		41.77	43.16	51.81
	D5cc ≤ 45Gy	38.71		33.79	39.26	43.11
	D0.5cc ≤ 39Gy		16.62			
LungGTV	D10% ≤ 20Gy	5.66	5.23	8.14	12.83	9.11
Spinalcord	Dmax ≤ 28Gy	13.10		5.61	16.15	12.09
	D0.35cc ≤ 22Gy	11.69		4.66	15.3	10.97

Compiled by the author

2.1.2. Planning features for the stereotactic technique with MRI-linac

With the exception of the second case, which used coplanar 15 static fields, the IMRT plans had 18 static coplanar fields, the majority of which were focused on the right side (nearer to the tumor) in order to maximize treatment and create a more uniform dose distribution (Fig. 7). For lung cases I and III-V, the gantry rotated counterclockwise from 22° to 181° and from 160° to 40°, leaving a 20-degree angle between each beam (plan extent from 0° to 340°). For lung case treatment II, the gantry rotated clockwise from 0° to 205° and from 220° to 340°.

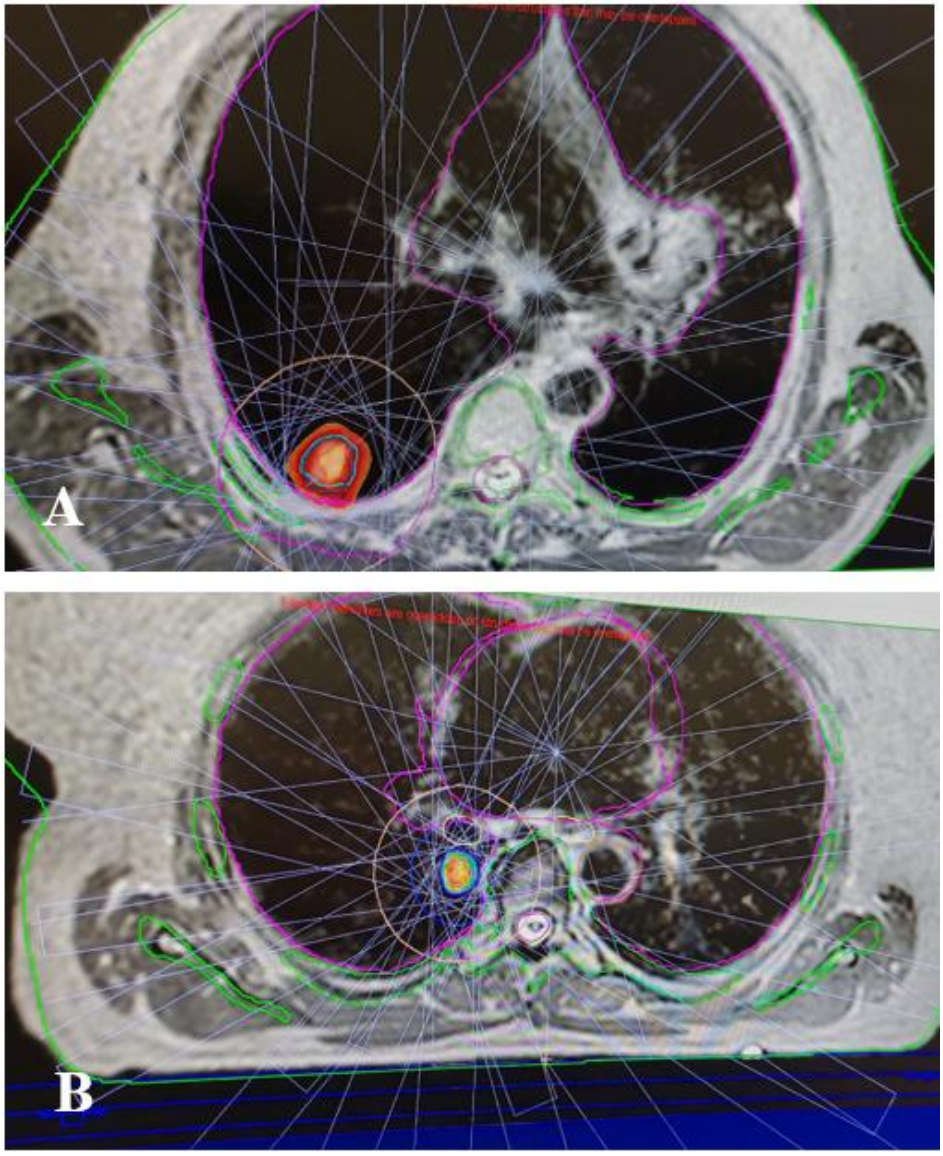

Fig. 7. Lung SBRT MRI-LINAC plan field configuration: A—Case I (18 fields), B—Case II (15 fields)

Table 5 summarizes the volumetric features of the target tissues and organs at risk in each of the five lung treatment cases included in this investigation. Significant interpatient heterogeneity is observed, reflecting variations in tumor size and anatomy.

The gross tumor volume ranges from 1.02 cc to 56.99 cc, while the PTV varies from 3.58 cc to 87.66 cc. Compared with the previous examples, the fourth case shows significantly greater target volumes, suggesting a more complicated treatment scenario. In all cases, the PTV is consistently larger than the GTV, reflecting the application of margins to account for setup uncertainties and inevitable motion.

Regarding normal tissue structures, the lung volumes (excluding GTV) show notable variation, ranging from approximately 2469 cc to over 5000 cc, which may influence dose distribution. The chest wall volumes also differ significantly between cases; Case IV once more has the

highest capacity (186.83 cc), which may affect dose restrictions and plan optimization. Similar anatomical representation in the field of therapy is suggested by the generally constant volumes of other organs at risk, such as the spinal cord. On the other hand, because of variations in tumor location and anatomical coverage, tissue like the liver is only present in certain instances.

Table 5. Volume of structures in each MRI-LINAC lung case (compiled by the author)

Structure	Case I	Case II	Case III	Case IV	Case V
	Volume (cc)				
PTV (or REGISTRATION)	10.11	3.58	19.15	87.66	20.19
GTV/CTV (or TARGET)	4.25	1.02	6.63	56.99	7.23
Bones	923.14	1270.99	1304.26	1031.95	1160.59
Chest wall	86.56	12.48	74.94	186.83	111.34
Lung-GTV	5069.76	2655.84	2962.15	2469.12	2746.73
Lungs	5074.01	2656.86	2968.79	2520.30	2753.92
Liver			1096.44	1525.48	1340.76
Spinal cord	55.12	35.98	21.71	19.28	22.03

Compiled by the author

Monitor units per fraction (MU / Fx) (Table 6) shows significant variation between lung cases, reflecting variations in modulation and plan complexity. In MRI-guided radiotherapy, where treatment duration affects intrafraction motion, certain cases show significantly higher MU values, which could indicate enhanced beam modulation due to stricter OAR constraints or improved PTV coverage. The increase in MU is also influenced by the target area, whose electron density is close to that of air, which is closely related to the challenge of lung planning. On the other hand, simpler treatment plans with less modulation can be represented by lower MU values.

Table 6. Comparison of monitor units per fraction in lung MRI-LINAC cases

MU/Fx				
Case I	***Case II***	***Case III***	***Case IV***	***Case V***
210.80	290.88	58.55	138.75	58.55
34.03	160.83	88.19	26.03	88.19
368.68	268.68	291.09	83.26	291.09
136.13	251.45	168.27	78.48	168.27
194.69	205.67	214.33	54.29	214.33
162.21	162.53	241.60	168.20	241.60
160.33	82.88	338.61	299.73	338.61
247.86	89.66	245.70	80.61	245.70
462.46	137.58	75.77	135.50	75.77
85.48	100.81	354.83	194.3	354.83
121.55	239.41	163.85	94.10	163.85
105.39	235.76	134.87	79.44	134.87
126.87	213.22	265.94	73.97	265.94
170.35	139.54	33.12	110.54	33.12
70.51	240.81	72.51	225.10	72.51
152.22		201.02	164.38	201.02
258.22		177.83	155.13	177.83
206.98		60.07	106.62	60.07

Compiled by the author

Table 7 reveals gathered anatomical and planning structure relative ED values, which are relevant in the dose calculation process. However, each planned case differed in the extent of relative electron density (ED) determination because the target volume size and anatomical position within the lung varied between cases. Certain organs at risk were not included in the ED analysis when they were located outside the clinically significant irradiation region or were not expected to receive relevant radiation exposure during treatment.

Table 7. Relative electron density for MRgART plan dose calculation

Structures	Relative ED				
	Case I	*Case II*	*Case III*	*Case IV*	*Case V*
Bones	1.173	1.218	1.140	1.152	1.146
Chest wall	0.995	1.029	0.993	1.033	0.954
Lungs		0.316	0.283	0.292	0.296
Spinal cord	1.032	1.089	1.043	1.073	
Esophagus		1.010			
Great vessels		1.012			
Heart		0.994			
Liver			1.044	0.965	0.959
GTV (or CTV)		0.499	1.00	0.821	
PTV	0.650	0.650	0.650	0.650	0.650

Compiled by the author

2.2. 4-D-CT- guided lung SBRT research methodology and methods

Two radiotherapy plans, created for a 6 x MeV photon beam in Varian Eclipse 16.1 software and intended for use with a TrueBeam STx linear accelerator, were assessed for CT-guided SBRT evaluation. The beams were planned for delivery using the VMAT technique, and dose calculation was performed with the Acuros XB algorithm. These therapy cases analyze a tumor located in the periphery of the right lung that followed the same dosimetric guidelines. A 5 mm PTV margin from the CTV (or GTV) was included in the lung treatment regimens.

To implement this method, infrared marker or surface-guidance tracking is used to manage the respiratory cycle by following chest wall mobility. Amplitude-based active gating (during the stable exhalation phase) was combined with a 4D-CT-based planning technique to account for respiratory motion during SBRT.

2.2.1. Clinical constraints for 4D-CT-based SBRT plans

Both curative treatment plans differed in total dose: in the first Case, 60 Gy was planned in 8 fractions (7.5 Gy / Fx), and in the second, 50 Gy in 5 fractions (10 Gy / Fx). Because the second Case received a higher dose than the first, the clinical constraints are stricter. Therefore, without changing the planning results achieved, both cases are analyzed according to the OAR constraints of the second lung treatment case (Table 8).

Table 8. Results of clinical constraints for the lung SBRT 4D-CT-LINAC plans

Clinical constraints		**I Case**	**II Case**
		Dose or coverage / gradient metric	
PTV	Dmax < 125%	113.14%	105.54%
	D95% ≥ 95%	95.42%	99.92%
	D99% ≥ 90%	91.64%	98.66%
	Gradient Measure ≥ 0.9 cm	1.37 cm	1.23 cm
	Gradient Measure ≤ 1.5 cm	1.37 cm	1.23 cm
	Conformity Index < 1.20	0.77	0.95
Bronchus_R	D0.5cc < 32 Gy	0.59 Gy	22.93 Gy
Lung-GTV	V20 < 10%	5.82%	8.61%
Esophagus	D0.5cc < 32 Gy	10.88 Gy	9.70 Gy
Heart	D0.5cc <27 Gy	14.35 Gy	14.26 Gy
Spinalcord	D0.1cc < 23 Gy	16.09 Gy	11.65 Gy
Chestwall	Dmax < 68 Gy	67.19 Gy	
	D30cc < 45 Gy	32.16 Gy	

Compiled by the author

2.2.2. Planning features for the stereotactic technique with 4D-CT-LINAC

4D-CT-guided stereotactic treatments were planned using coplanar VMAT with two partial arcs (Fig. 8): a clockwise 181°-0° arc paired with a counterclockwise 0°-181° arc to minimize low-dose exposure to healthy tissues. Each partial arc was created of 90 segments; in the first Case, the clockwise arc is equal to 1100.9 MU, when the counterclockwise arc is 1176.4 MU, and in the second Case, 1506.8 MU and 1462.3 MU, respectively.

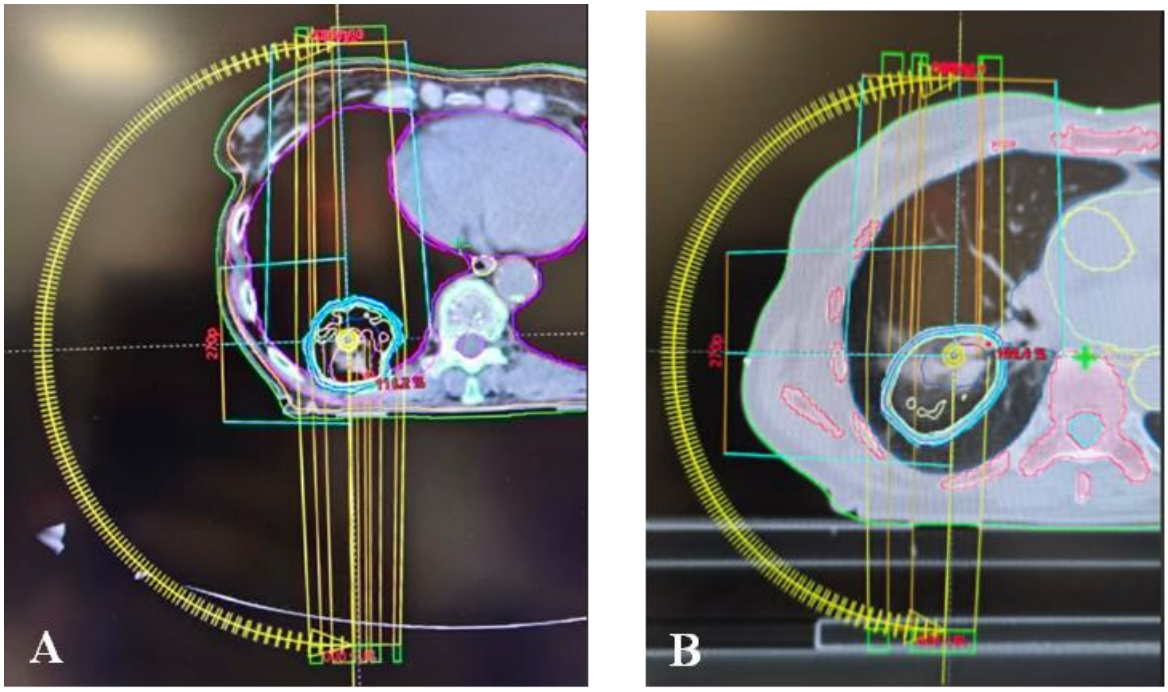

Fig. 8. 4D-CT-guided SBRT planning: A – Case I (standard CT window display), B – Case II (lung CT window display)

Both the initial tumor size and the subsequent extension to the PTV differ between cases (Table 9). The gross tumor volume in Case I is significantly higher at 36.9 cc, more than double the 16.6 cc seen in Case II. In the first treatment plan, the PTV increased from GTV doubling to 73.8 cc, and in the second, it increased almost 2.8 times (62.7 cc).

Table 9. Volume of structures in the 4D-CT-LINAC lung case

Structure	Case I	Case II
	Volume (cc)	
GTV (or CTV)	36.9	16.6
PTV	73.8	62.7

Compiled by the author

2.3. Research methodology and methods on statistical modulation of PTV

To evaluate the impact of GTV and the selected margin size on PTV outcome, five abstract treatment plans for a middle lung tumor were selected for statistical modulation analysis: MRgART (coded as “MRI”), 4D-CT-guided SBRT (“SBRT1”, “SBRT2”) with amplitude gathing, and conventional approaches (3D-CT-based) with and without breathing management (respectively, “conWith” and “conWithout”) (Table 10). Structure delineation for MR-guided treatment was performed using the Monaco 6.2.2.0 treatment planning system for an Elekta Unity 1.5 T MR-Linac; for 4D-CT-guided and conventional methods, Varian Eclipse 16.1 was used for a TrueBeam STx linear accelerator. The same two margin sizes from the GTV were

applied to all plans: 5 and 10 mm. These margin sizes were applied to the sagittal, longitudinal, and transverse axes.

Table 10. Volume (cc) of structures for statistical modulation analysis

Method	GTV	PTV (margin of 5 mm)	PTV (margin of 10 mm)
Stereotactic MRgART (MRI)	0.69	5.25	16.80
4D-CT-based SBRT (SBRT1)	4.25	15.30	36.10
4D-CT-based SBRT (SBRT2)	6.63	21.90	48.70
Conventional without breathing control (conWithout)	57.97	119.00	198.00
Conventional with breathing control (conWith)	7.14	26.70	59.20

Compiled by the author

For statistical modulation result evaluation, the absolute change (4), relative change (5), expansion ratio (6), and relative dispersion (7) were calculated by formulas:

$$\Delta V = V_{(10\ mm)} - V_{(5\ mm)}; \quad (4)$$

$$\Delta V(\%) = \frac{V_{(10\ mm)} - V_{(5\ mm)}}{V_{(5\ mm)}} \times 100; \quad (5)$$

$$\frac{PTV_{(5\ mm\ or\ 10\ mm)}}{GTV}; \quad (6)$$

$$CV = \left(\frac{\sigma}{\mu}\right) \times 100\ \%; \quad (7)$$

where CV is the coefficient of variation, σ is the standard deviation, and μ is the mean.

2.4. Research limitations

The same lung treatment case was not used and analyzed between treatment methods in this study; all treatment plans were distinguished by gross tumor volume and treatment outcome - PTV and the corresponding achieved clinical constraints results. The ITV planning parameter was removed from the study in order to lower uncertainty and enhance comparability between treatment plans resulting from various ITV determination techniques during respiratory motion management in both conventional radiotherapy and 4D-CT-based SBRT. Moreover, due to the limited scope of treatment plans for the 4D-CT-guided SBRT method (two lung treatment cases), it was not possible to use correlation and regression analyses.

For statistical modulation, an abstract comparison of PTV between the four radiation treatment methods was feasible with only one or two (4D-CT-guided SBRT) cases for comparison, showing how sensitively the PTV result changes depending on the selected margin size, regardless of the prescribed dose, fraction size, or gross tumor volume.

2.5. Results of the examination

2.5.1. Analysis of the PTV dependency in lung MR-LINAC plans

Relation between GTV and PTV

The scatter plot (Fig. 9) demonstrates the inseparable relation between GTV and PTV. There is a strong positive linear trend (R = 0.995), with PTV volume rising in direct proportion to GTV volume. The fitted regression line closely follows the distribution of data points, indicating a consistent and predictable relationship across all cases. However, this relationship is intrinsically important for treatment outcome. While excessively broad margins increase the volume of healthy tissue irradiated, thereby increasing toxicity and perhaps limiting dose delivery, inadequate margins may lead to treatment delivery misses and decreased tumor control [49]. Therefore, to ensure adequate coverage of the target while reducing normal tissue exposure, an ideal balance is needed, which is frequently achieved through customized margin design based on tumor motion and imaging accuracy, according to Trémolières et al. [58].

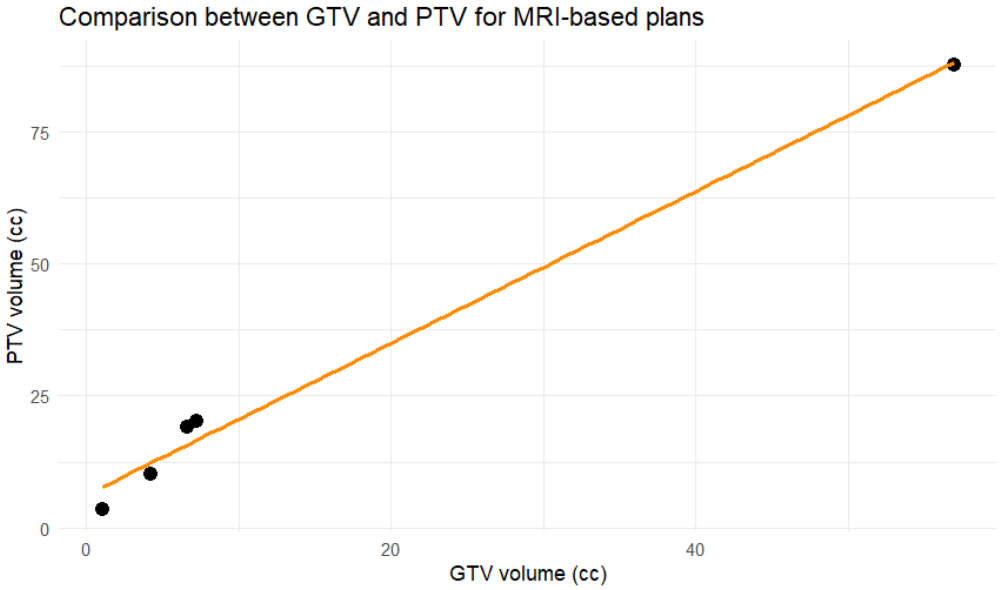

Fig. 9. Scatter plot of GTV and PTV relation (created by the author)

The extent of the PTV margin relative to the gross tumor volume across five lung cases is depicted in the bar chart in Figure 10. Compared to the other lung treatment cases, the fourth Case has the largest margin extension (around 30.7 cc), which is much greater and is associated with the largest GTV (56.99 cc), compared to other tumor cases in this dataset, which range from 1.02 cc to 7.23 cc. Case II, on the other hand, exhibits the lowest margin volume (2.557 cc), indicating a more constrained GTV to PTV expansion. The margin volumes in the remaining examples (I, III, and V) are intermediate, ranging from 5.861 cc to 12.961 cc. This difference implies that margin expansion varies among individual cases within the tumor volume and cancerous spread around the visible cancer growth.

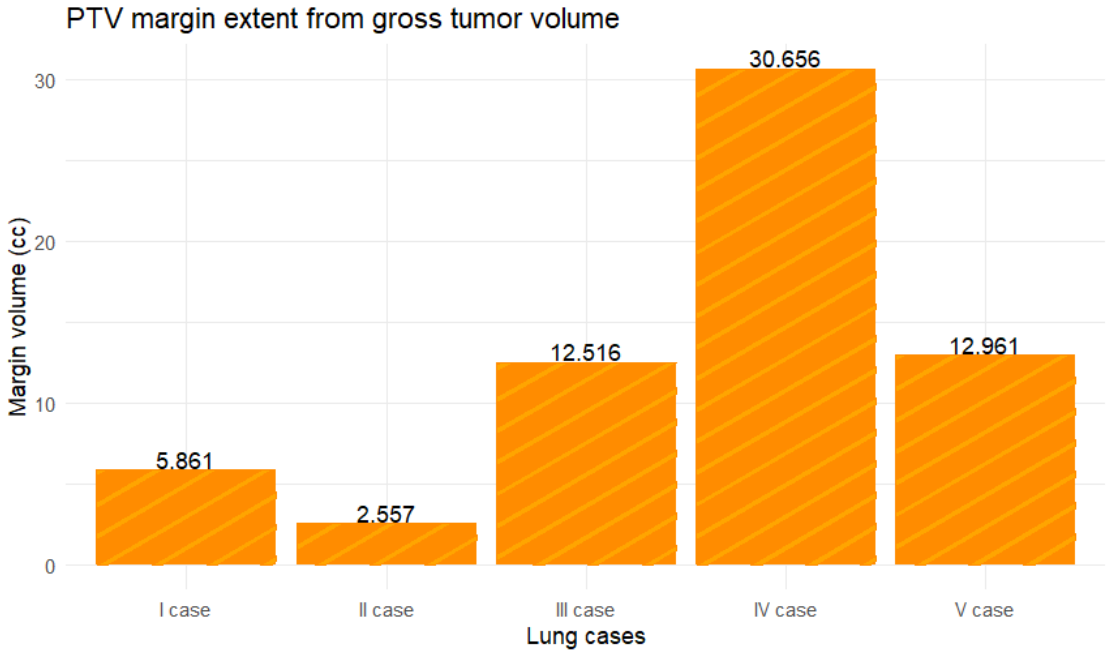

Fig. 10. PTV margin extends from the GTV in MRI-LINAC plans (created by the author)

Comparison of the achieved target coverage

The boxplot shows abstract PTV coverage metrics ($D_{98\%}$, $D_{99\%}$, and D_{max}) across the five lung cases due to a small sample size (Fig. 11). Even though the constraints are grouped by type, slightly different clinical dose criteria were applied for each case (e.g., $D_{max} \leq 48$ Gy (+2 Gy) was applied to Case II, but for Cases III and IV, $D_{max} \leq 44$ Gy (+2 Gy) was adjusted). The PTV constraint of D_{max} exhibits the highest coverage values, followed by $D_{98\%}$. In contrast, the $D_{99\%}$ constraint was applied only to one case (Case II, corresponding to the treatment of the smallest lung tumor (GTV = 1.02 cc) among the other cases), yielding a dose of approximately 38 Gy.

The volume of $D_{98\%}$ ranges from 38.7 Gy (Case IV, whose limit is 39.5 cc, almost meets the minimum volume limit) to 49.2 Gy. Cases I and V are very close to the maximum constraint limit, equal to 49.16 Gy and 49.23 Gy, respectively. However, $D_{98\%}$ has an outlier Case III (PTV = 38.70 Gy), which is almost at the minimum volume limit. This demonstrates the flexibility of SBRT planning, which balances clinically acceptable minimum coverage criteria with target dose escalation, as indicated by the broader distribution of achieved coverage metrics.

Accordingly, D_{max} is characterized by higher dose coverage than the other discussed PTV constraints, which range from 42.8 Gy to 54.4 Gy, indicating that hotspot intensity increases more noticeably than overall target coverage. Cases III and IV are very close to the minimum dose limit, at 42.92 Gy and 42.80 Gy, respectively, with the maximum limit reached in Case V (52.63 Gy) and the median in Case II (45.52 Gy). However, an outlier also emerged, which corresponds to case I (54.45 Gy).

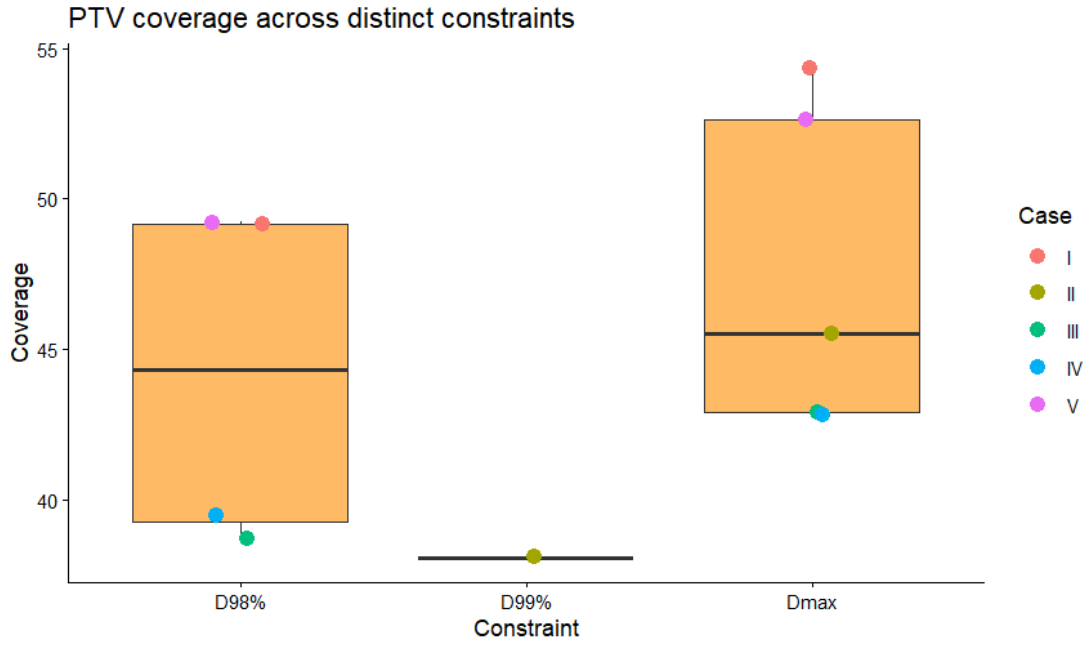

Fig. 11. Boxplot of PTV coverage among different PTV constraints (created by the author)

Relation between target coverage and clinical constraints

Strong and moderate correlations between several clinical dosage limits and PTV coverage parameters are shown in the Spearman method correlation matrix (Fig. 12). The correlation heatmap reveals a strong positive correlation between D_{max} and $chestwall_{Dmax}$ (R = 0.80), as well as between $D_{98\%}$ and both $chestwall_{Dmax}$ and $chestwall_{D5cc}$ (R = 0.80). This suggests that increased dose to the chest wall is associated with improved PTV coverage, indicating a potential trade-off between target dose escalation and chest wall sparing. Conversely, there is a significant negative association (R = -0.80) between D_{max} and lung-GTV, suggesting that greater lung dosage limitations may restrict the maximum dose that can be administered to the PTV. This illustrates how treatment planning is affected by lung protection regulations.

For most variables, the spinal cord restrictions ($spinalcord_{Dmax}$ and $spinalcord_{D0.35cc}$) exhibit weak to moderately positive correlations (R = -0.20–0.40), indicating a relatively little impact on PTV coverage in these lung treatment cases. Furthermore, several clinical constraints limit themselves to exhibiting moderate correlations, such as between $chestwall_{D5cc}$ and lung-GTV (R = 0.60), suggesting dependency between various anatomical dosage limitations. Therefore, carefully avoiding the one clinical constraint may also affect the dose to the other organ at risk and PTV coverage.

Overall, the results suggest that clinical limitations, particularly those related to the lungs and chest, have direct implications for PTV coverage. The findings highlight how crucial it is to balance organ-at-risk protection with sufficient target coverage when selecting a course of treatment.

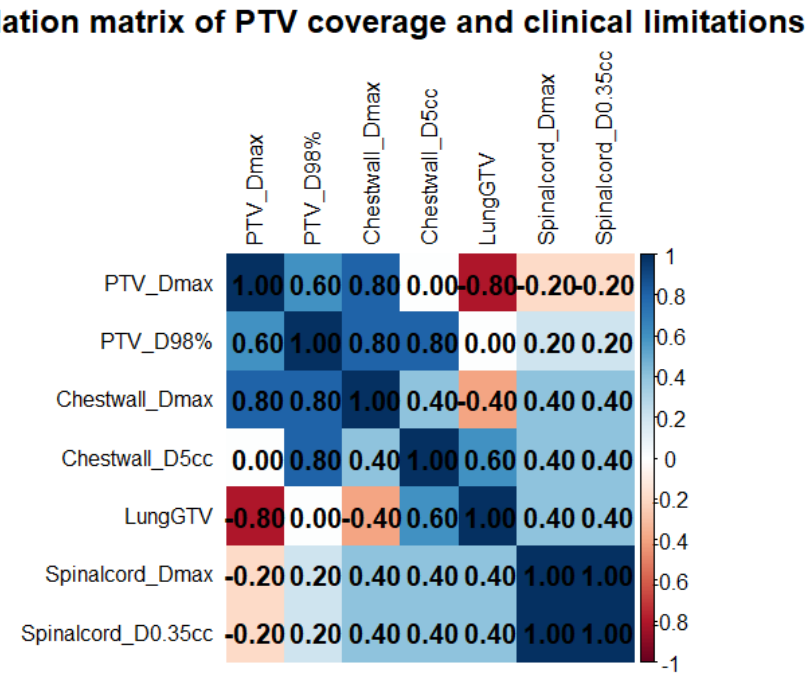

Fig. 12. Correlation heatmap of PTV and OAR clinical limitations in lung MRgART (created by the author)

Additionally, a linear regression analysis was performed to evaluate the relationship between PTV dose (D_{max} / $D_{98\%}$) and clinical constraints ($chestwall_{Dmax}$ and lung-GTV were the only significant ones). Among the models with D_{max}, $chestwall_{Dmax}$ demonstrated a significant positive correlation ($\beta = 0.994$, $p = 0.007$), indicating that higher chest wall doses are associated with higher maximum doses within the PTV (1% significance level). Lung-GTV, with the same model, on the other hand, showed a significant negative connection ($\beta = -0.304$, $p = 0.044$), suggesting that the attainable maximum dosage to the target volume may be limited by more restrictive lung-dose constraints (5% significance level). Thus, tight lung dose constraints appear to limit dose escalation within the PTV coverage goal, whereas less restrictive chest wall constraints may permit higher PTV doses.

Relative electron density across anatomical structures

The distribution of relative electron density values across thoracic anatomical structures is shown in the boxplot in Figure 13. There are noticeable variations in electron density among tissues, reflecting their different physical compositions.

Due to its air-filled composition, the lungs showed the lowest relative electron density values (around 0.28–0.32). These findings are consistent with research by Mihailidis et al. [37], which reported an average lung electron density of 0.30 relative to water. However, the lung relative electron density value in the boxplot (Fig. 13) was removed as an outlier to reveal the relationship and arrangement of the values of other anatomical structures with each other. Bones, on the other hand, exhibit the greatest electron density values (about 1.14–1.22), which might be affected by mineral content. Additionally, the spinal cord exhibits values marginally

higher than those of other soft tissues but remains within a narrow range of 1.03–1.09, closer to bone relative ED results. Still, for instance, Brevitt et al. [6] demonstrate that dense bone elements can achieve a relative electron density of up to approximately 1.46 (compared with 1.12 for trabecular bone).

The electron density values of soft tissues, such as the liver (approximately 0.96–1.04), heart (0.99), chest wall (about 0.99–1.03), esophagus (1.01), and major vessels (1.01), are very similar and typically cluster around unity, which is closer to water equivalence. This suggests that there are only slight differences in the radiological characteristics of these tissues. This RED value pattern around 1 is evident in the research by Brevitt et al. [6], where soft tissue ranges from 0.976 (breast) to 1.043 (muscle) to 1.052 (liver).

However, clear separation between low-density (lungs), intermediate-density (soft tissues), and high-density (bone) structures highlights the heterogeneity of thoracic tissues. These diversities are clinically considerable, as variations in electron density directly influence dosage estimation and radiation attenuation in treatment planning.

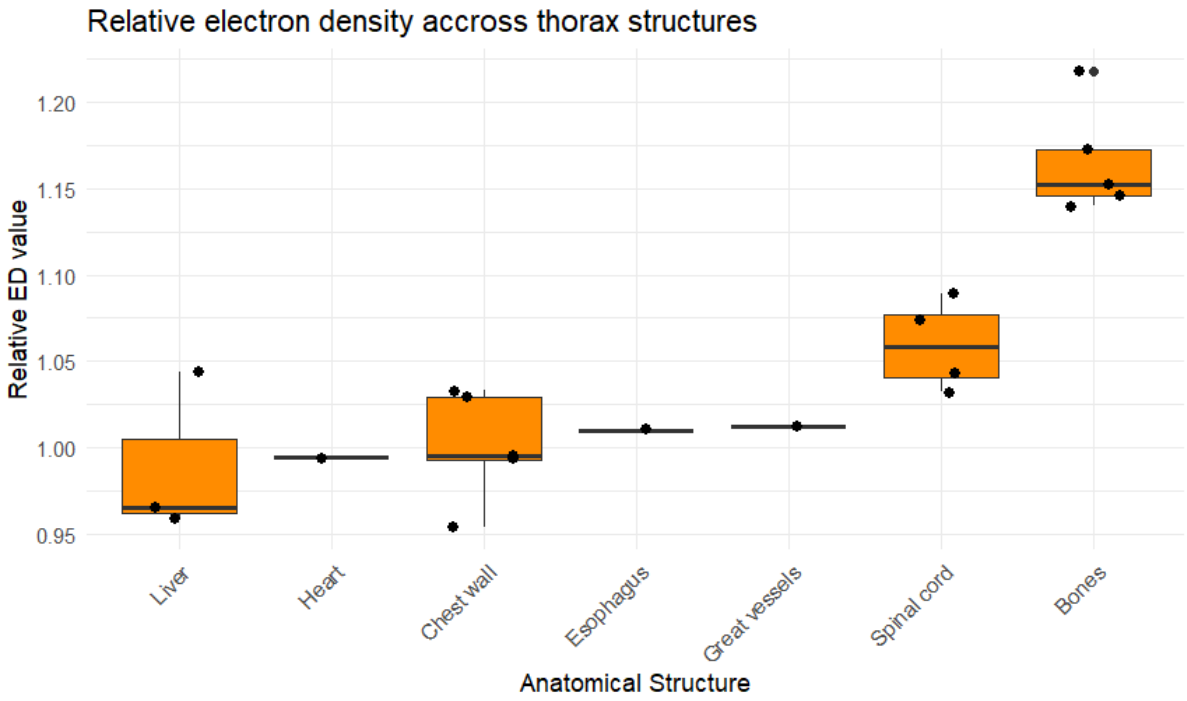

Fig. 13. Relative ED across thorax structures (created by the author)

2.5.2. Analysis of the PTV dependency in lung 4D-CT-LINAC plans

Volume change between GTV and PTV

In 4D-CT-guided SBRT planning for two lung cancer cases with the same 5 mm expansion margin, the resulting margin volumes reached 36.9 cc in Case I and 46.1 cc in Case II, despite the same margin application. The higher growth volume seen in Case II could be related to

variations in the target geometry, which result in an irregular, elongated PTV shape, to the initial tumor size (16.6 cc), or even target placement, closer to the lung middle.

Comparison of the achieved target coverage

The distribution of important dosimetric PTV constraints ($D_{95\%}$, $D_{99\%}$, and D_{max}) across the assessed CT-guided SBRT instances is depicted in Figure 14. Notably, Case II continuously shows better coverage than Case I for both the $D_{95\%}$ and $D_{99\%}$ metrics, indicating a more stable dose distribution throughout the target volume. In these instances, the average coverage for $D_{95\%}$ and $D_{99\%}$ is 97.67% and 95.15%, respectively. Additionally, target coverage values of $D_{99\%}$ were lower than $D_{95\%}$, which could reflect the increased difficulty of maintaining near-complete dose coverage throughout the entire PTV. Although all D_{max} values remained below the clinical limit of 125%, the maximum dose outcomes showed the greatest variability. Compared with Case II, Case I showed a slightly higher D_{max}, which could account for a slightly less uniform dose distribution within the target volume. This is also reflected in the conformity index, which is 0.77 for Case I (0.95 for Case II). Nevertheless, the differences observed were not clinically relevant and remained acceptable.

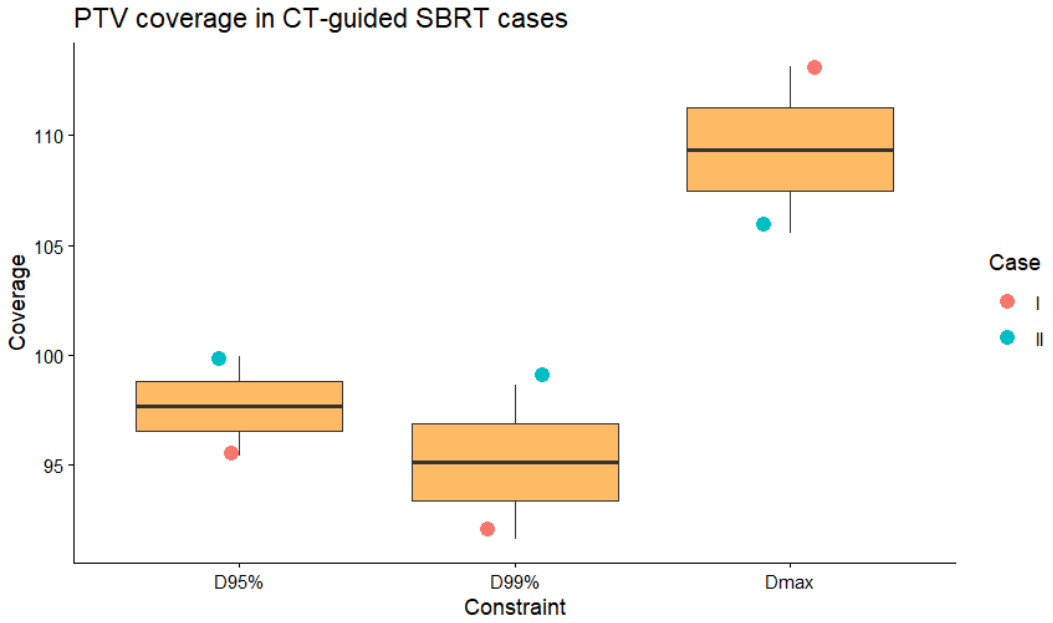

Fig. 14. Boxplot of PTV coverage among different PTV constraints in 4D-CT-guided SBRT (created by the author)

Relation between target coverage and clinical constraints

Notwithstanding the drawbacks of the small sample size, which could result in statistically unstable correlation coefficients, an abstract trend of relationship can be observed between PTV coverage parameters and OAR clinical constraints in the Spearman correlation matrix (Fig. 15). The coverage metrics $D_{95\%}$ and $D_{99\%}$ show a negative correlation with D_{max}. This shows that the target volume's overall coverage results in a reduction as the plan gets "hotter" (i.e., with a higher maximum dose). A positive correlation between $D_{95\%}$, $D_{99\%}$ PTV coverage

parameters, and lung-GTV (also bronchus constraint) could imply that expanding the target coverage near the tumor's edge, the "coolest" areas of the PTV, directly raises the dose delivered to the surrounding lung tissue. Additionally, a positive association between D_{max} and organs such as the heart, esophagus, and spinal cord is seen in the correlation heatmap. The relationship suggests that the dose to healthy organs is far more affected by the radiation plan's maximum intensity (the "hot spots") than by how well the radiation actually covers the tumor.

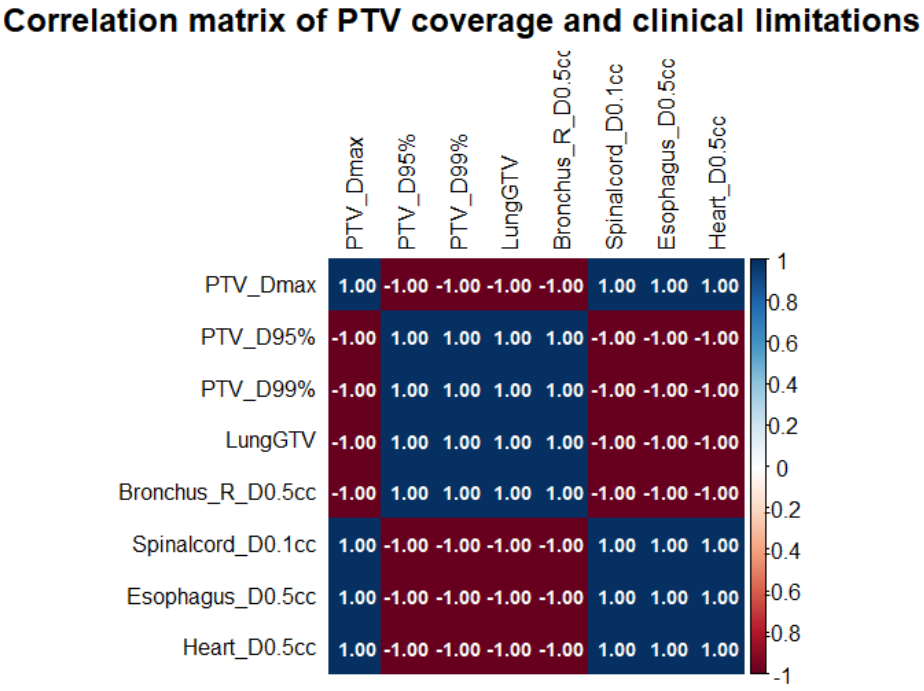

Fig. 15. Correlation heatmap of PTV coverage and OAR clinical limitations in 4D-CT-guided SBRT treatments (created by the author)

For both 4D-CT-based SBRT cases, Table 11 shows the relative organ-at-risk dose ratios to various PTV coverage metrics. In comparison to Case II, Case I continuously showed lower ratio values for lung-GTV across all assessed PTV coverage measures. The lung-to-coverage ratios ranged from 0.0514 to 0.0635 in Case I and from 0.0816 to 0.0873 in Case II. This implies that, while maintaining sufficient target coverage, Case I achieved comparatively better sparing of healthy lung tissue. Spinal cord dosage ratios showed a similar trend, with Case II showing marginally lower values than Case I across all assessed coverage criteria. Relatively similar dose relationships for these organs-at-risk were indicated by the esophageal and cardiac ratios, which only slightly differed between the two cases. Even though only Case I's chest wall relative ratios were known, the obtained values remained relatively constant across several PTV coverage criteria.

Table 11. Relative ratio between organs-at-risk and PTV coverage parameter

PTV coverage metric	Case	Organs-at-risk relative ratios					
		LungGTV	**Chest wall (D_{max})**	**Chest wall (D_{30cc})**	**Spinal cord**	**Esophagus**	**Heart**
D_{max}	I	0.051	0.594	0.284	0.142	0.096	0.127
	II	0.082			0.110	0.092	0.135
$D_{95\%}$							
	I	0.061	0.704	0.337	0.169	0.114	0.150
	II	0.086			0.117	0.097	0.143
$D_{99\%}$							
	I	0.064	0.733	0.351	0.176	0.119	0.157
	II	0.087			0.118	0.098	0.145

Compiled by the author

2.5.3. Statistical PTV modulation of the margin expansion effect

Comparison of volume change to form PTV among different radiotherapy methods

The statistical modulation of the volumetric impact of PTV formation was assessed by adding 5 mm and 10 mm margins from the GTV across different lung SBRT and conventional treatment-contouring methods. The findings, compiled in Table 12, show that switching from a 5 mm to a 10 mm margin, the conventional approach without breathing control indicated the largest absolute volume increase, by 78.8 cc. However, this technique has the smallest relative rise, at only 66.39%, suggesting that greater baseline volumes can be more stable in percentage terms. On the other hand, the stereotactic MRgART technique's relative volume increased by 220%, even though its absolute rise was the lowest at 11.5 cc. This demonstrates a geometric dependency in radiation planning: small target volumes experience exponential relative growth, which could greatly raise the dose to nearby healthy lung tissue. Additionally, the relative expansion characteristics of the conventional (with breathing control) and CT-based SBRT approaches were consistent.

Table 12. Statistical modeling comparison of PTV size between lung radiotherapy methods

Method	**GTV**	**PTV (margin of 5 mm)**	**PTV (margin of 10 mm)**	**Absolute change (cc) / Relative change (%)**	**Expansion ratio from GTV to PTV with a 5 mm / 10 mm margin**
MRI	0.693	5.25	16.80	11.50 / 220.00	7.58 / 24.19
SBRT1	4.247	15.30	36.10	20.80 / 135.95	3.60 / 8.50
SBRT2	6.634	21.90	48.70	26.70 / 122.37	3.30 / 7.34
conWithout	57.972	119.00	198.00	78.80 / 66.39	2.06 / 3.42
conWith	7.141	26.70	59.20	32.60 / 122.72	3.73 / 8.29

Compiled by the author

The bar graph in Fig. 16 shows a notable difference in the responses of several contouring techniques to margin expansions. The most sensitive approach to the margin expansion is the stereotactic MRgART method, which achieves an expansion value of 24.19 at a 10 mm verge, more than double the 7.58 at a 5 mm margin. The expansion patterns of conventional (with respiratory motion control) and CT-based guided SBRT techniques are quite comparable; their expansion values fall between 7.34 and 8.50 at 10 mm and between 3.30 and 3.73 at 5 mm. However, with a ratio of just 3.42 at a 10 mm margin, the conventional (without breathing control) approach exhibits the lowest expansion values.

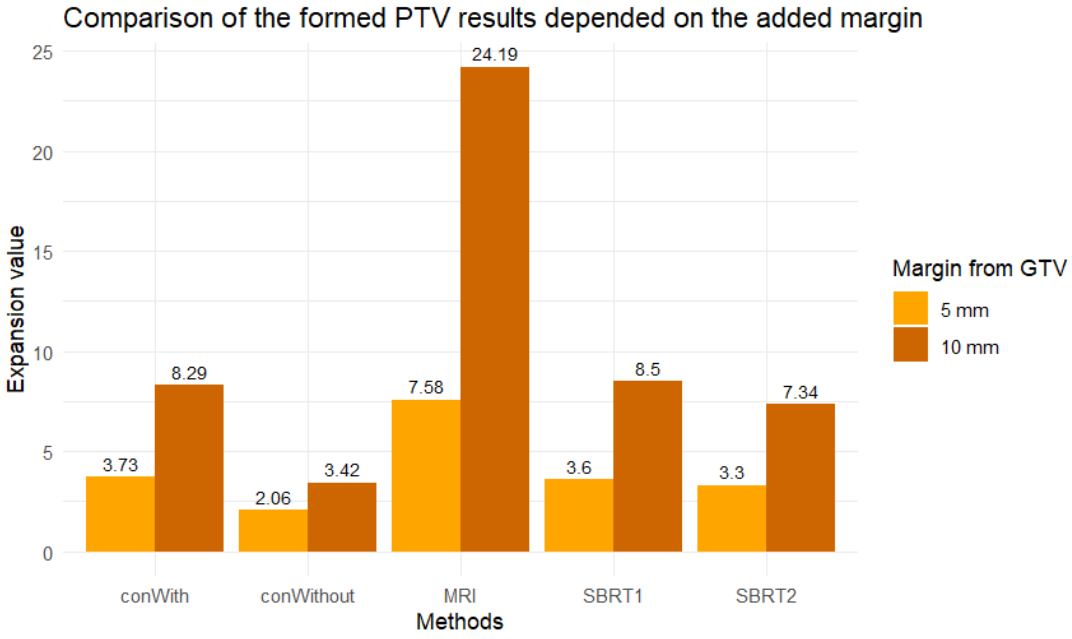

Fig. 16. PTV formation and comparison between lung radiotherapy methods (created by the author)

To ascertain the relative dispersion of expansion ratios in this statistical model, the coefficient of variation was calculated using all technique expansion ratios from GTV to the formed PTV with a 5 and 10 mm verge. The tight clustering of data points within the interquartile ranges in a boxplot examination of expansion ratios (Fig. 17) indicates great consistency across most contouring techniques. Only two notable exceptions stand out: the conventional method without breathing control showed lower ratios due to its comparatively large baseline volume, whereas the adaptive MR-based method showed very high ratios due to its small-volume sensitivity. Furthermore, all technique verge expansion ratios are quite similar at 5 mm, but the variations between techniques become significantly more pronounced and scattered when the margin is changed to 10 mm. The expansion ratio with a 5 mm mean value is 4.06, the standard deviation is 2.08, and reaches 51.30 of CV. When at a 10 mm margin, the expansion ratio's mean value reaches 10.30, standard deviation of 8.01, and CV increases to 77.40. This abrupt increase in CV indicates that as the margin increases, the PTV growth across approaches widens and becomes less predictable.

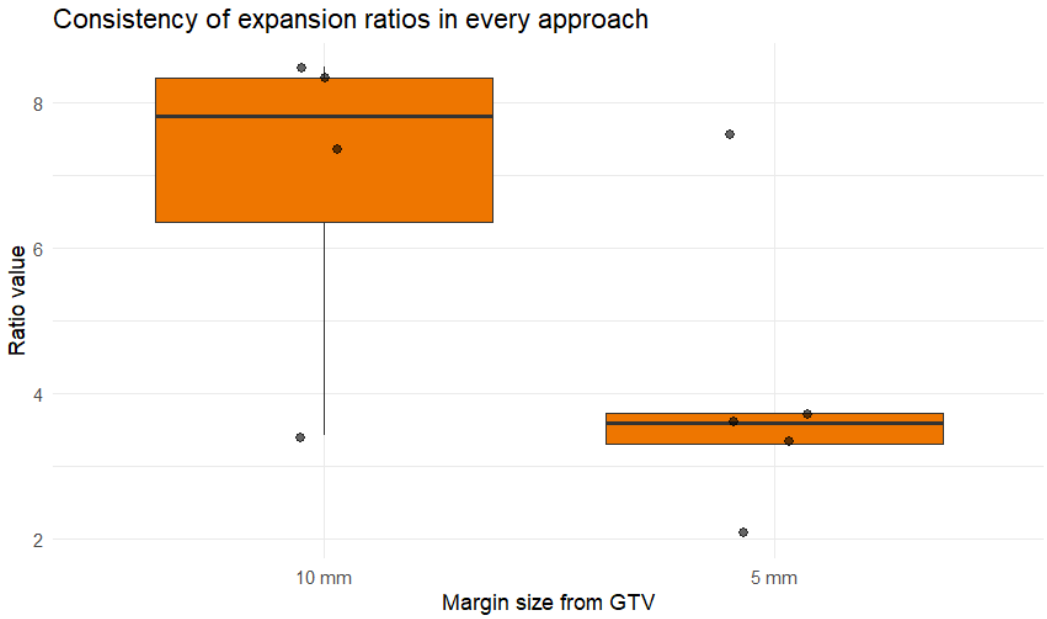

Fig. 17. Expansion ratio from GTV to PTV consistency determination boxplot without MRgART outlier value at 10 mm margin (created by the author)

Additionally, the planned target volumetric impact of margin expansion from 5 to 10 mm across lung radiotherapy techniques was assessed using a paired t-test. The results showed that the p-value of 0.044 is lower than the significance level of 0.05, so it can be claimed that volume had increased statistically significantly. A mean volume increase of 34.08 cc (95% CI: 1.59, 66.57) was the average outcome of the 10 mm verge.

Also, the non-parametric test of the Wilcoxon was used for PTV difference analysis. Although the results reveal a difference that is not statistically significant ($p = 0.0625$), this value, which may have been attenuated by the small sample size, shows a tendency toward increased volume with a 1 cm margin compared to 0.5 cm.

Despite a tendency observed in statistical testing, the effect size was negligible (Cohen's $d = 0.06$), indicating that the difference between margins is not clinically relevant. After excluding an outlier (adaptive MR-based SBRT method), a small effect size (Cohen's $d = 0.25$) emerged, suggesting a possibly hidden underlying difference. However, the impact of individual cases highlights the dataset's unpredictability.

Comparison of PTV volume change patterns

Finally, to find commonalities among all treatment techniques, Principal Component Analysis (PCA) was used. The horizontal axis (PC1 of 82.38%) is dedicated to the difference in volume size between radiotherapy methods, whereas the vertical axis (PC2 of 17.6%) shows the residual variance, in this case, the PTV expansion sensitivity. In Figure 18, clustering between 4D-CT-based SBRTs and conventional (with respiratory management) technique cases was found in the analysis, indicating that these techniques yield greatly consistent volumetric results. On the other hand, the stereotactic MRgART and conventional (without breathing

control) approaches were outliers, indicating the extremes of small-volume sensitivity and large-volume stability, respectively.

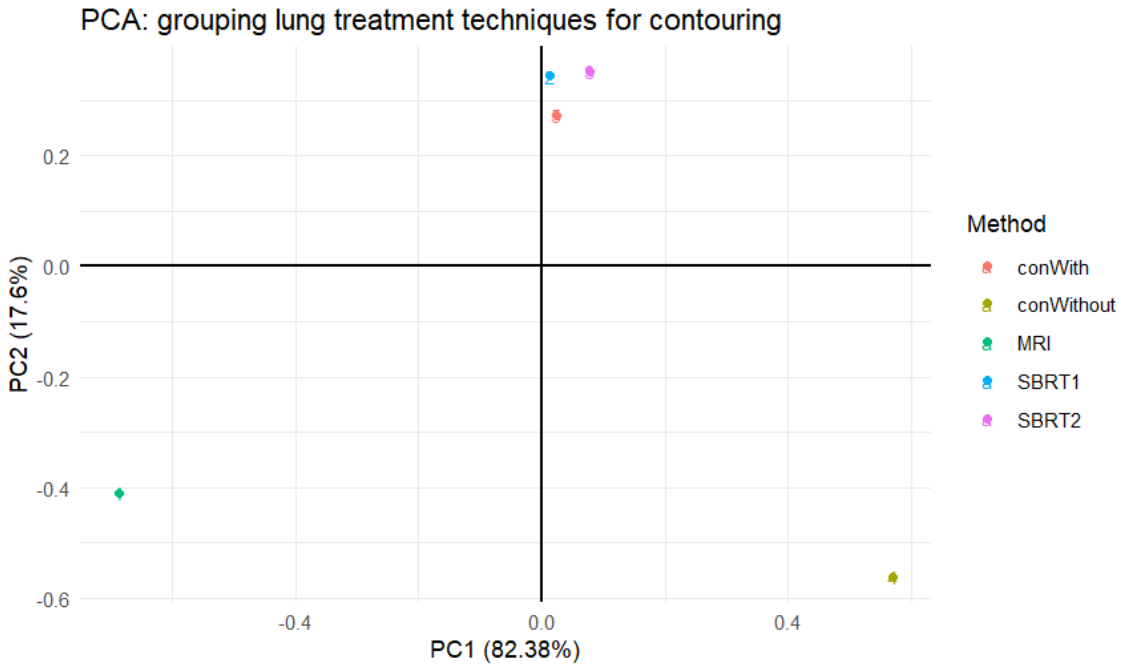

Fig. 18. Principal component analysis of PTV fluctuation due to the margin size (created by the author)

2.5.4. Discussion of results

This study's results enable discussion of factors, such as margin size, conformity index, and clinical constraint trade-offs, that determine treatment outcome. Comparison between stereotactic methods and dose-volume metrics has been complicated by differing implied clinical criteria, which are more stringent in the magnetic resonance-guided adaptive radiotherapy strategy. This is most evident between the chest wall and spinal cord clinical criteria: maximum dose to the chest wall is equal to or lower than 57 Gy in MRgART stereotactic method, when 4D-CT based technique allows up to 68 Gy dose; spinal cord dose for a larger volume is lower ($D_{0.35cc} \leq 22$ Gy) in MRgART than for a smaller volume of OAR ($D_{0.1cc} < 23$ Gy) in CT-guided stereotactic strategy. Additionally, the observed associations and trends should be interpreted as exploratory rather than definitive clinical conclusions, given the small sample size of this study, especially for 4D-CT-guided SBRT.

2.5.4.1. Gross tumor volume and margin size influence on treatment outcome

This study showed that the initial tumor volume and motion-management method, in addition to the applied geometric margin, have a substantial impact on PTV formation. The resulting volumetric expansion varied notably, even though the same margin size was used in multiple methods. This impact was particularly pronounced in stereotactic MRgART, where relative PTV increases were achieved with extremely small target volumes. Comparing stereotactic methods

planned with the same 5 mm margin, the margin-influenced expansion ratio for the stereotactic MRgART method ranges from 1.5 to 2.9, while the 4D-CT-based SBRT method achieves an expansion ratio of 2 to 3.8. However, these results are inextricably influenced by the gross tumor volume, which in the analyzed CT-guided SBRT method was larger than in the stereotactic MRgART lung treatment cases (e.g., 16.6 cc and 7.23 cc, respectively). Also, taking into account the statistical modulation result, MRgART showed a difference of 3.2 times between the margin changes from 10 to 5 mm, while the result of CT-guided SBRT was 2.2 to 2.4 times (corresponding to the conventional method with respiratory control), and the conventional technique without respiratory control showed a 1.7 expansion ratio. These results highlight the geometric sensitivity of stereotactic radiation treatment planning and underscore the need for customized margin selection based on respiratory motion, imaging accuracy, tumor size, and tumor location within the lungs. Munshi et al.'s [38] study measured the effect of margin expansions on target size. The research found a particular correlation: when the initial target is small, even a little uniform expansion (such as a few millimeters) leads to a significant increase in the overall volume that must be irradiated [38]. The findings in this study align with Munshi et al.'s [38] inference that relative volume change is the most important aspect for moving targets with a narrow radius, even though the absolute volume change is greater for larger tumor targets.

Additionally, the excessive volume expansion can unnecessarily increase irradiation of healthy lung tissue despite the use of advanced image-guiding and motion monitoring; this phenomenon may be clinically important. As the tumor volume reduces, the margin, rather than the tumor itself, becomes the primary determinant of how much healthy lung tissue is exposed to radiation. Hoffman et al. [24] found that PTV size significantly affects clinically feasible dose gradients and lung SBRT conformity. This investigation confirmed the strong geometric dependence of stereotactic planning by demonstrating that increasing PTV volume modifies dose falloff characteristics and effects surrounding normal tissue exposure [24].

Furthermore, the extraordinarily small gross tumor volume (0.693 cc) of the stereotactic MRgART plan analyzed in statistical modulation reveals the advantage of MRI-guided visualization during treatment delivery. A recent study by Corradini et al. [11] emphasizes that the MRgART method is highly effective, demonstrating the capability to treat incredibly small lung targets, including gross tumor sizes as small as 0.5 cc. According to this scientific article, even for ultracentral thoracic lesions near important anatomical structures, MRgART permitted great conformal dose distribution while upholding organ-at-risk limitations. These findings show that MRI-guided systems can safely irradiate exceptionally small tumor targets that would be challenging to follow and locate using conventional CT-based image-guided LINAC methods due to breathing aberrations, lower soft-tissue contrast, and limited temporal resolution.

2.5.4.2. Clinical target coverage trade-off with organs at risk

Although the lung treatment plans investigated did not exceed the established clinical guideline limits in this study, the analysis suggests an inherent trade-off between optimal target coverage and sparing of organs at risk. Two structures - chest wall and lung-GTV - showed the most

pronounced dependence of the dose received on PTV coverage in correlation and linear regression methods.

Improved target coverage may come at the cost of higher dose deposition in nearby normal tissues, as evidenced by strong positive relationships between PTV coverage measurements and chest wall dose. This dependence also defines Leung et al. [33] because, when adding a PTV constraint to account for detection and mobility errors, the high-dose region naturally extends into nearby normal structures such as the chest or ribs, and strong positive correlations are observed. Additionally, Fink et al. [15] showed that robustly optimized plans considerably decreased thoracic wall hotspot dosages ($D_{0.05cc}$).

On the other hand, negative correlations between PTV dose and lung-GTV constraints suggest that stricter lung sparing may prevent dose escalation within the target volume. This relationship was also observed in the scientific paper by Bryant et al. [7] for more restrictive lung-sparing clinical goals (e.g., V20). Leung et al. [33] state that in order to preserve acceptable lung dosage metrics, optimization algorithms may restrict beam intensity and decrease internal hotspot development.

In the analysis results, it can be observed that the spinal cord MRgART method shows a weak positive correlation with PTV coverage $D_{98\%}$, which directly affects both: as coverage increases, spinal cord dose increases as well. However, the spinal cord has a negative correlation with the maximum dose. This finding suggests that increases in hotspot intensity within the target volume were not associated with increased spinal cord dose. However, in the CT-based SBRT analysis, the maximum dose shows a positive correlation trend with the spinal cord, esophagus, and heart, whereas $D_{95\%}$ and $D_{99\%}$ coverage indicate a negative relationship. The maximum dose within the treatment plan is often more strongly associated with OAR dose escalation than with improvements in target coverage itself, according to a study by Murrell et al. [39] on thoracic SBRT optimization. Ultracentral lung SBRT frequently requires purposefully compromising PTV coverage to maintain doses to the spinal cord, bronchial tree, esophagus, and heart within clinically acceptable tolerances [39].

2.5.4.3. Significance of conformity index and hotspot behavior

Treatment plan quality is often assessed using dosimetric metrics such as the conformance index and maximum dose, which reflect dose heterogeneity and hotspot formation within the PTV. The compliance condition of CI < 1.20 was met by both 4D-CT-guided SBRT treatment plans. In comparison to Case I (CI = 0.77), Case II showed better conformance (CI = 0.95), suggesting that the prescription isodose more closely matched the PTV geometry. In contrast, the lower conformity observed in Case I may reflect a less homogeneous dose distribution and greater dose spillage outside the target volume. Both treatment regimens, however, stayed within clinically acceptable bounds. In both situations, the maximal dose within the PTV stayed below the recognized SBRT threshold of 125%. In contrast to Case II (105.54%), Case I showed a larger hotspot (113.14%), indicating a somewhat more varied dosage distribution. However, because controlled dose heterogeneity within the target may improve dose falloff and organ-at-

risk sparing, hotspot levels are accepted in lung SBRT planning, given the lungs' low-density structure, according to Bryant et al. [7].

The conformity indices ranged from 0.70 to 0.86, with Case II exhibiting the highest conformance, in MR-guided adaptive SBRT plans. Although a higher maximum dose in the planning result (as in Cases I and V, equal to 54.35 Gy and 52.63 Gy, respectively) may indicate lower plan homogeneity, the electron return effect can influence both the maximum dose and the overall homogeneity profile, which is explained in Andreozzi et al.'s [1] study. This phenomenon results in local dose enhancement and the formation of hotspots, which raise the maximum dose and decrease dose homogeneity, especially near tissue–air interfaces such as the lung, skin, and air cavities [1].

2.5.4.4. Target volumetric comparison between motion-managed approaches

Variations in the planning target volume size between the assessed treatment techniques were shown by the statistical modeling study. The conventional approach with breathing control resulted in a 74.5% increase in PTV volume compared with the first 4D-CT SBRT case. Similarly, when the second 4D-CT SBRT lung case was used as the reference, the PTV volume increased by 21.9% with the conventional radiotherapy technique. These statistically modulated PTV results comparing the conventional and stereotactic approaches with respiratory management differ a little from the Nyman et al. [42] study, which found that the SBRT method reduced PTV by 58.9% in a randomized study. However, this difference in results could be due to the small sample size of this study.

One important result of this statistical modeling is that the geometric expansion dynamics of 4D-CT SBRT and conventional motion-managed methods differ dramatically, even when using the same radial margin across highly comparable baseline target volumes. The scientific study by Wei et al. [60] distinguishes dose sparing in normal tissues due to target dosage heterogeneity. In their research, it was claimed that the stereotactic technique allows for a much quicker dose fall-off just outside the target periphery, thereby reducing lung tissue irradiation and benefiting from regulated internal heterogeneity [60]. Therefore, these results show that SBRT does more than just achieve tighter volumes through improved imaging; its underlying radiobiological planning principle significantly modifies three-dimensional dose scaling, enabling better sparing of normal lung tissue even with the same structural margins. On the other hand, a more uniform dosage distribution throughout the target is a prerequisite for a conventional motion-managed approach. Planning optimization must enlarge the physical PTV footprint by extending the high-dose limits outward to achieve this conformity.

Conclusions

1. Respiratory motion management is essential in lung radiotherapy to reduce geometric uncertainty and planning target volume margins (from 3 to 5 mm compared with conventional method margins of 5 to 20 mm), while improving dosimetric accuracy. Techniques such as 4D-CT, respiratory gating, and MR-guided adaptive radiotherapy enhance target precision. Advanced dose calculation algorithms, including Monte Carlo and Acuros XB, improve dose modeling in heterogeneous lung tissue and may affect dose conformity and organ-at-risk sparing.
2. The chest wall and lung-GTV showed the strongest relationship between dose exposure and planning target volume coverage ($R = 0.80$ and $R = -0.80$, respectively, when $\beta = 0.994$, $p = 0.007$ between maximum dose and chest wall, $\beta = -0.304$, $p = 0.044$ with lung-GTV), particularly in peripheral tumors. Improved target coverage was associated with higher chest wall dose, while more restrictive lung sparing limited dose escalation within the target volume.
3. Statistical modulation revealed that motion-managed conventional and 4D-CT-guided stereotactic strategies exhibit more similar margin expansion patterns within the planned target volume. In contrast, the MR-guided adaptive stereotactic method showed the highest sensitivity to margin expansion. This illustrates a geometric dependency in radiation planning: smaller target volumes experience exponential relative growth, which could significantly increase the dosage to adjacent healthy lung tissue, whereas larger tumor targets experience greater absolute volume change.

References

1. ANDREOZZI, J. M., BRŮŽA, P., CAMMIN, J., POGUE, B. W., GLADSTONE, D. J., & GREEN, O. Optical imaging method to quantify spatial dose variation due to the electron return effect in an MR-linac. *Medical Physics*, *47*(3), 1258–1267, 2019. Access via: https://doi.org/10.1002/mp.13954
2. ASLAN, D. & AKSOZEN, M. T. Dosimetric comparison of IMRT, VMAT, and hybrid techniques in stereotactic body radiotherapy for adrenal metastases. *Scientific Reports, 15(1), 20623,* 2025. Access via: https://doi.org/10.1038/s41598-025-06707-1
3. BARSKY, A. R., KIM, M. M., MAXWELL, R., MENDES, A. et al. Initial clinical experience treating patients with palliative radiotherapy for malignant pleural mesothelioma on the HalcyonTM linear accelerator. *Annals of Palliative Medicine, 9(5), 2903–2912*, 2020. Access via: https://doi.org/10.21037/apm-20-385
4. BEZJAK, A., PAULUS, R., GASPAR L. E., R. D. TIMMERMAN et al. Safety and efficacy of a Five-Fraction stereotactic body radiotherapy schedule for centrally located Non–Small-Cell lung cancer: NRG Oncology/RTOG 0813 trial. *Journal of Clinical Oncology, 37*(15), 1316–1325, 2019. Access via: https://doi.org/10.1200/jco.18.00622
5. BISELLO, S., CILLA, S., BENINI, A., CARDANO, R., NGUYEN, N. P. et al. Dose–Volume Constraints for Organs At Risk In Radiotherapy (CORSAIR): An “All-in-One” Multicenter– Multidisciplinary Practical Summary. *Current Oncology, 29(10), 7021–7050*, 2022. Access via: https://doi.org/10.3390/curroncol29100552
6. BREVITT, B. A., SUAREZ, E. G., CLEMENTE, R. A. M., & VOUTCHKOV, M. Evaluating the impact of CT scanning parameters on dose calculations by the treatment planning system in external beam radiation therapy. *Journal of Cancer Therapy and Research*, *1*(1), 2021. Access via: https://doi.org/10.52793/jctr.2021.1(1)-08
7. BRYANT, J. M., SIM, A. J., FEYGELMAN, V., LATIFI, K., & ROSENBERG, S. A. Adaptive hypofractionted and stereotactic body radiotherapy for lung tumors with real-time MRI guidance. *Frontiers in Oncology*, *13*, 1061854, 2023. Access via: https://doi.org/10.3389/fonc.2023.1061854
8. CHOW, J. C. H., LUI, J. C. F., TONG, C. K. C., TAM, A. H. P., CHAN, J. C. H. et al. Efficacy and safety of high-dose hypofractionated palliative radiotherapy (40 Gy in 10 daily fractions) for non–small cell lung cancer. *Radiation Oncology Journal*, *43*(4), 188–194, 2025. Access via: https://doi.org/10.3857/roj.2025.00346
9. CHUA, G. W. Y., & CHUA, K. L. M. Which patients benefit most from stereotactic body radiotherapy or surgery in medically operable non-small cell lung cancer? An in-depth look at patient characteristics on both sides of the debate. *Thoracic Cancer, 10*(10), 1857–1867, 2019. Access via: https://doi.org/10.1111/1759-7714.13160
10. CIRINO, E., BENEDICT, S. H., DUPRE, P. J., HALVORSEN, P. H., G. G. KIM et al. AAPM-RSS Medical Physics Practice Guideline 9.b: SRS-SBRT. *Journal of Applied Clinical Medical Physics*, *26*(4), e14624, 2025. Access via: https://doi.org/10.1002/acm2.14624
11. CORRADINI, S., ALONGI, F., ANDRATSCHKE, N., BELKA, C., BOLDRINI, L. et al. MR-guidance in clinical reality: current treatment challenges and future perspectives.

Radiation Oncology, *14*(1), 92, 2019. Access via: https://doi.org/10.1186/s13014-019-1308-y

12. CSIKI, E., SIMON, M., PAPP, J., BARABÁS, M., J. MIKÁCZÓ et al. Stereotactic body radiotherapy in lung cancer: a contemporary review. *Pathology & Oncology Research, 30,* 2024. Access via: https://doi.org/10.3389/pore.2024.1611709
13. Das, I. J., Alongi, F., Yadav, P., & B. B. Mittal. (2024). *A practical guide to MR-Linac*. Springer: Cham, Switzerland, 71-73, 84-85, 2024. Access via: https://doi.org/10.1007/978-3-031-48165-9
14. ELCIM, Y. Effects of electron density force to 1.0 and fill to 1.0 on VMAT treatment plans for lung SBRT. *Journal of Applied Clinical Medical Physics*, *25*(10), e14488, 2024. Access via: https://doi.org/10.1002/acm2.14488
15. FINK, T. L., KRISTIANSEN, C., HANSEN, T. S., HANSEN, T. F., & THING, R. S. Robust optimization of the Gross Tumor Volume compared to conventional Planning Target Volume-based planning in photon Stereotactic Body Radiation Therapy of lung tumors. *Acta Oncologica*, *63*, 448–455, 2024. Access via: https://doi.org/10.2340/1651-226x.2024.40049
16. FOGLIATA, A., NICOLINI, G., A. CLIVIO et al. Dosimetric evaluation of Acuros XB Advanced Dose Calculation algorithm in heterogeneous media. *Radiation Oncology, 6*(1), 82, 2011. Access via: https://doi.org/10.1186/1748-717x-6-82
17. FROMETA-CASTILLO, T., PYAKURYAL, A., WALS-ZURITA, A. & A. MESBAHI. (2020). Biologically Effective dose (BED) or radiation Biological Effect (RBEF)? In IntechOpen eBooks. Access via: https://doi.org/10.5772/intechopen.92029
18. GHANI M. N. H. A., & W. L. NG. Management of respiratory motion for lung radiotherapy: a review. *Journal of Xiangya Medicine,* 2018. Access via: https://doi.org/10.21037/jxym.2018.06.03
19. GLIDE-HURST C. K., I. J. CHETTY. Improving radiotherapy planning, delivery accuracy, and normal tissue sparing using cutting edge technologies. Journal Of Thoracic Disease, 6(4), 2014. Access via: https://doi.org/10.3978/j.issn.2072-1439.2013.11.10
20. GROSU A., NIEDER C., N. H. NICOLAY. Target volume Definition in radiation Oncology. *Springer, Cham*, 115–145 p., 2023. Access via: https://doi.org/10.1007/978-3-031-45489-9
21. GUTIÉRREZ, E., SÁNCHEZ, I., DÍAZ, O., VALLES, A., R. BALDERRAMA et al. Current Evidence for Stereotactic Body Radiotherapy in Lung Metastases. *Current Oncology, 15*;28(4):2560–2578, 2021. Access via: doi: 10.3390/curroncol28040233
22. HAN, E. Y., YEBOA, D. N., BRIERE, T. M., YANG, J., & WANG, H. Dosimetric analysis of MR-LINAC treatment plans for salvage spine SBRT re-irradiation. *Journal of Applied Clinical Medical Physics*, *23*(10), e13752, 2022. Access via: https://doi.org/10.1002/acm2.13752
23. HEALY, G. E. A., MARSH, S. H., & COUSINS, A. T. The dosimetric effect of electron density overrides in 3DCRT Lung SBRT for a range of lung tumor dimensions. *Journal of Applied Clinical Medical Physics*, *19*(6), 79–87, 2018. Access via: https://doi.org/10.1002/acm2.12446

24. HOFFMAN, D., DRAGOJEVIĆ, I., HOISAK, J. et al. Lung Stereotactic Body Radiation Therapy (SBRT) dose gradient and PTV volume: a retrospective multi-center analysis. *Radiat Oncol* 14, 162, 2019. Access via: https://doi.org/10.1186/s13014-019-1334-9
25. HSU, S., ZAWISZA, I., O'GRADY, K., PENG, Q., & TOMÉ, W. A. Towards abdominal MRI-based treatment planning using population-based Hounsfield units for bulk density assignment. *Physics in Medicine and Biology*, *63*(15), 155003, 2018. Access via: https://doi.org/10.1088/1361-6560/aacfb1
26. HWANG, U., MIN, B. J., KIM, M., & K. KIM. Image guided radiation therapy. *Progress in Medical Physics, 33*(4), 37–52, 2022. Access via: https://doi.org/10.14316/pmp.2022.33.4.37
27. IBA Dosimetry. Normal tissue constraints for SRS / SBRT. 2021. Access via: https://www.ibadosimetry.com/fileadmin/user_upload/products/02_radiation_therapy/myqa_srs/iba_dose _contraints_poster_rev2_0522.pdf. [looked 2025-12-5]
28. INTERNATIONAL ATOMIC ENERGY AGENCY. *Absorbed Dose Determination in External Beam Radiotherapy An International Code of Practice for Dosimetry Based on Standards of Absorbed Dose To Water.* Vienna: Technical Reports Series No. 398 (Rev. 1), 2024. Access via: https://doi.org/10.61092/iaea.ve7q-y94k
29. Joe, Y., Chang, L., Dong, H., Liu, G., Starkschall et al. Image–Guided Radiation Therapy for Non–Small Cell Lung Cancer. *Journal of Thoracic Oncology, 3*(2), 177-186 pages, 2008. Access via: https://doi.org/10.1097/JTO.0b013e3181622bdd
30. KATZ L. M., NG V., WU S. P., YAN S., GREW D. et al. Stereotactic body radiation therapy for the treatment of locally recurrent and oligoprogressive Non-Small cell lung cancer: a single institution experience. *Frontiers in Oncology, 12,* 2022. Access via: https://doi.org/10.3389/fonc.2022.870143
31. KHAN, A. M. H., HASHMI, S. F. A., LI, B., SHAUKAT, F., Y. AHMED et al. Stereotactic radiotherapy: An educational narrative review. *Precision Radiation Oncology, 8*(1), 47–58, 2024. Access via: https://doi.org/10.1002/pro6.1222
32. LEE, M., YOON, K., CHO, B., KIM, S. S., S. Y. SONG et al. Comparing phase‐ and amplitude‐gated volumetric modulated arc therapy for stereotactic body radiation therapy using 3D printed lung phantom. *Journal of Applied Clinical Medical Physics, 20*(2), 107–113 p., 2019. Access via: https://doi.org/10.1002/acm2.12533
33. LEUNG, R. W. K., CHAN, M. K. H., CHIANG, C., WONG, M., & BLANCK, O. On the pitfalls of PTV in lung SBRT using type-B dose engine: an analysis of PTV and worst case scenario concepts for treatment plan optimization. *Radiation Oncology*, *15*(1), 130, 2020. Access via: https://doi.org/10.1186/s13014-020-01573-9
34. LI C., WANG L., WU Q., ZHAO J., YI F. et al. A meta-analysis comparing stereotactic body radiotherapy vs conventional radiotherapy in inoperable stage I non-small cell lung cancer. *Medicine, 99*(34), e21715, 2020. Access via: https://doi.org/10.1097/md.0000000000021715
35. MENTEN, M. J., FAST, M. F., NILL, S., KAMERLING, C. P., MCDONALD, F. et al. Lung stereotactic body radiotherapy with an MR-linac – Quantifying the impact of the magnetic

field and real-time tumor tracking. *Radiotherapy and Oncology*, *119*(3), 461–466, 2016. Access via: https://doi.org/10.1016/j.radonc.2016.04.019
36. MEYERS, S. M., KISLING, K., ATWOOD, T. F., X. A. RAY. Standardized workflow for respiratory-gated motion management decision-making. *Journal of Applied Clinical Medical Physics, 23*(8), 2022. Access via: https://doi.org/10.1002/acm2.13705
37. MIHAILIDIS, D., TSAPAKI, V., & TOMARA, P. A simple manual method to estimate water-equivalent diameter for calculating size-specific dose estimate in chest computed tomography. *British Journal of Radiology*, *94*(1117), 20200473, 2020. Access via: https://doi.org/10.1259/bjr.20200473
38. MUNSHI, A., SARKAR, B., PAUL, S., CHAUDHARI, B. B., CHAUHAN, R. S. et al. A mathematical formulation for volume expansions in contouring for radiotherapy planning. *Journal of Cancer Research and Therapeutics*, *17*(4), 1125–1131, 2021. Access via: https://doi.org/10.4103/jcrt.jcrt_614_19
39. MURRELL, D. H., LABA, J. M., ERICKSON, A., MILLMAN, B., PALMA, D. A., & LOUIE, A. V. Stereotactic ablative radiotherapy for ultra-central lung tumors: prioritize target coverage or organs at risk? *Radiation Oncology*, *13*(1), 57, 2018. Access via: https://doi.org/10.1186/s13014-018-1001-6
40. NAGATA Y., & T. KIMURA. Stereotactic body radiotherapy for lung cancer: a review. *Japanese Journal of Clinical Oncology*, 55(12), 1316–1325, 2025. Access via: https://doi.org/10.1093/jjco/hyaf142
41. NG, J., GREGUCCI, F., PENNELL, R. T., NAGAR, H., E. B. GOLDEN et al. MRI-LINAC: A transformative technology in radiation oncology. *Frontiers in Oncology*, *13*, 1117874, 2023. Access via: https://doi.org/10.3389/fonc.2023.1117874
42. NYMAN J., HALLQVIST A., LUND J., BRUSTUGUN O., BERGMAN B., BERGSTRÖM P. et al. SPACE – A randomized study of SBRT vs conventional fractionated radiotherapy in medically inoperable stage I NSCLC. *Radiotherapy and Oncology, 121(1),* 1–8, 2016. Access via: https://doi.org/10.1016/j.radonc.2016.08.015
43. PRUNARETTY J., BOISSELIER P., AILLÈRES N., O. RIOU et al. Tracking, gating, free-breathing, which technique to use for lung stereotactic treatments? A dosimetric comparison. *Reports of Practical Oncology & Radiotherapy, 24*(1), 97-104 p., 2019. Access via: https://doi.org/10.1016/j.rpor.2018.11.003
44. QIAO, Q., ZHU, W., TIAN, C., SHI, X., P. XIE et al. (2025). Real-time magnetic resonance imaging guided accelerator in stereotactic body radiation therapy for non-small cell lung cancer. *Journal of Thoracic Disease*, *17*(7), 5055–5064, 2025. Access via: https://doi.org/10.21037/jtd-24-686
45. REGNERY, S., BUCHELE, C., WEYKAMP, F., POHL, M., P. HOEGEN et al. Adaptive MR-Guided Stereotactic Radiotherapy is Beneficial for Ablative Treatment of Lung Tumors in High-Risk Locations. *Frontiers in Oncology*, *11*, 757031, 2022. Access via: https://doi.org/10.3389/fonc.2021.757031
46. REVERBERI, C., & M. TROVÒ. Stereotactic radiotherapy for early-stage non-small cell lung cancer. *Mini-invasive Surgery,* 2020. Access via: https://doi.org/10.20517/2574-1225.2020.33

47. RRAKAQI, B., TELHAJ, E., ELEZAJ, N., KAÇIU, Y., XHAFA, B. et al. Evaluation of Hounsfield numbers and electron density for a CT simulator and their importance for radiotherapy treatments. *International Journal of Biomedicine*, *15*(2), 2025. Access via: https://doi.org/10.21103/article15(2)_oa14
48. RUGGIERI, R., BIANCHI, N., GURRERA, D., NACCARATO, S., R. F. BORGESE. et al. Validation of a Monte Carlo-based dose calculation engine including the 1.5 T magnetic field for independent dose-check in MRgRT. *Physica Medica*, *130*, 104906, 2025. Access via: https://doi.org/10.1016/j.ejmp.2025.104906
49. SAVANOVIĆ, M., JAROŠ, D., & J. FOULQUIER. Planning target volume density impact on treatment planning for lung stereotactic body radiation therapy. *Acta Oncologica, 60*(10), 1296–1300, 2021. Access via: https://doi.org/10.1080/0284186x.2021.1950926
50. SCHMITT, D., BLANCK, O., GAUER, T., FIX, M. K., T. B. BRUNNER et al. Technological quality requirements for stereotactic radiotherapy. *Strahlentherapie Und Onkologie*, *196*(5), 421–443, 2020. Access via: https://doi.org/10.1007/s00066-020-01583-2
51. SHAO, K., CHEN, W., XU, Y., & S. YANG. Application of respiratory motion management technology for patients with lung cancer treated with stereotactic body radiotherapy (Review). *Oncology Letters*, *30*(3), 1–12, 2025. Access via: https://doi.org/10.3892/ol.2025.15161
52. SIEVINEN, J., ULMER W., W. KAISSL. *AAA Photon Dose Calculation Model in Eclipse*. Varian Medical Systems. Access via: https://tpswiki.com/wp-content/uploads/2022/01/AAAAlgorithm.pdf [looked 2026-03-08].
53. STECIW, S., FALLONE, B. G., & E. YIP, E. Dose perturbations at tissue interfaces during parallel linac-MR treatments: The “Lateral Scatter Electron Return Effect” (LS-ERE). *Medical Physics*, *51*(11), 8506–8523, 2024. Access via: https://doi.org/10.1002/mp.17363
54. TANAKA, H., ONO, T., UEDA, K., M. KARITA et al. Deep inspiration breath hold real-time tumor-tracking radiation therapy (DBRT) as a novel stereotactic body radiation therapy approach for lung tumors. *Scientific Reports, 14*(1), 2024. Access via: https://doi.org/10.1038/s41598-024-53020-4
55. THE ROYAL COLLEGE OF RADIOLOGISTS. *Radiotherapy dose fractionation: fourth edition.* Clinical Oncology, 2024. Access via: https://www.rcr.ac.uk/media/0d4mrqi5/radiotherapy-dose-fractionation-fourth-edition.pdf [looked 2026-03-08].
56. TIMMERMAN, R., PAULUS, R., J. GALVIN et al. Stereotactic Body Radiation Therapy for Inoperable Early Stage Lung Cancer. *JAMA, 303*(11):1070–1076, 2010. Access via: doi:10.1001/jama.2010.261
57. TORTORELLI, F., BORRAZZO, C., MASI, M., RAGO, M., R. E. GAWHARY et al. A quantification of the electron return effect using Monte Carlo simulations and experimental measurements for the MRI-linac. *Biomedical Physics & Engineering Express*, *11*(1), 015010, 2024. Access via: https://doi.org/10.1088/2057-1976/ad8ce3

58. TRÉMOLIÈRES P., GONZALEZ-MOYA A., PAUMIER A., MEGE M., J. BLANCHECOTTE et al. Lung stereotactic body radiation therapy: personalized PTV margins according to tumor location and number of four-dimensional CT scans. *Radiation Oncology, 17*(1), 2022. Access via: https://doi.org/10.1186/s13014-021-01973-5
59. WANG D., CHEN J., ZHANG X., ZHANG T. et al. Sparing Organs at Risk with Simultaneous Integrated Boost Volumetric Modulated Arc Therapy for Locally Advanced Non-Small Cell Lung Cancer: An Automatic Treatment Planning Study. Cancer Management and Research, Volume 12, 9643–9653, 2020. Access via: https://doi.org/10.2147/cmar.s273197
60. WEI, Z., PENG, X., WANG, Y., YANG, L., HE, L. et al. Influence of target dose heterogeneity on dose sparing of normal tissue in peripheral lung tumor stereotactic body radiation therapy. *Radiation Oncology*, *16*(1), 167, 2021. Access via: https://doi.org/10.1186/s13014-021-01891-6